J|A|C|S ARTICLES

Published on Web 01/27/2010

Orbital-Specific Energy Transfer

Troy E. Knight and James K. McCusker*

Department of Chemistry, Michigan State University, East Lansing, Michigan 48824

Received August 28, 2009; E-mail: jkm@chemistry.msu.edu

Abstract: The synthesis, structure, and photophysical properties of a new family of trinuclear $CuRe_2$ chromophore-quencher complexes having the general form $[Cu(pyacac)_2(Re(bpy')(CO)_3)_2](OTf)_2$ (where pyacac = 3-(4-pyridyl)-acetylacetonate and bpy′ = 4,4′-5,5′-tetramethyl-2,2′-bipyridine (tmb, **1**), 4,4′-dimethyl-2,2′-bipyridine (dmb, **2**), 2,2′-bipyridine (bpy, **3**), 4,4′-dichloro-2,2′-bipyridine (dclb, **4**), and 4,4′-diethylester-2,2′-bipyridine (deeb, **5**)) are reported. Time-resolved emission data acquired in room-temperature CH_2Cl_2 solutions revealed excited-state lifetimes of 14.9 ± 0.7, 8.1 ± 0.4, 8.2 ± 0.4, 5.6 ± 0.3, and 5.0 ± 0.3 ns for complexes **1**−**5**, respectively. The emission in each case is assigned to decay of the Re^{I}-based ^{3}MLCT excited state; the lifetimes are all significantly less than the corresponding $BeRe_2$ model complexes, which were also prepared and characterized. Electron transfer was found to be significantly endothermic for all five $CuRe_2$ complexes: this fact, coupled with the ca. 10 Å donor−acceptor distance and favorable spectral overlap between the ^{3}MLCT emission profile and absorptions of the Cu^{II} center, implicates dipolar energy transfer as the dominant quenching pathway in these compounds. Gaussian deconvolution of the ground-state absorption spectrum of $Cu(phacac)_2$ (phacac = 3-phenylacetylacetonate) allowed for a differential analysis of the spectral overlap between the donor emission spectra and the two observed ligand-field transitions of the Cu^{II} ion. Energy transfer was found to occur preferentially to the lower energy ligand-field band due primarily to more favorable dipole orientation as measured by the κ^2 term from Förster theory. These results, supported by time-dependent DFT calculations on $Cu(phacac)_2$, indicate enhanced dipolar coupling to the $d_{xz} \rightarrow d_{xy}$ transition of the Cu^{II} center and thus represent an orbitally specific energy-transfer process occurring in this system.

Introduction

The development of molecular assemblies that can serve as photoactive components of optical systems[1−9] requires exquisite control of their photophysical properties. This level of control, in turn, can only be achieved if the nature of the ground and excited states of the constituents can be elucidated.[10−12] Polypyridyl complexes of Re^{I}, Ru^{II}, Os^{II}, and Ir^{III} have received considerable attention in this regard due to their synthetic accessibility as well as the structure−function correlations that have emerged from several decades of research on their photoinduced properties.[13−24] As a result, compounds within this class have been utilized in a variety of settings ranging from fundamental studies of electron donor/acceptor interactions[25−32] to artificial photosynthetic systems[33−36] and, most recently, as catalysts for water splitting reactions.[37−40]

Recent work from our own group focused on energy transfer dynamics in a tetranuclear assembly consisting of three Re^{I} polypyridyl donors surrounding an $Fe^{III}(acac)_3$ moiety.[41] Emission from the Re^{I}-based ^{3}MLCT excited state was efficiently quenched by the Fe^{III} core; dipolar coupling between the Re^{I} fluorophore and absorptions associated with the Fe^{III} center was

(1) Balzani, V.; Credi, A.; Venturi, M. *Chem. Soc. Rev.* **2009**, *38*, 1542.
(2) Adronov, A.; Gilat, S. L.; Frechet, J. M. J.; Ohta, K.; Neuwahl, F. V. R.; Fleming, G. R. *J. Am. Chem. Soc.* **2000**, *122*, 1175.
(3) Cline, E. D.; Adamson, S. E.; Bernhard, S. *Inorg. Chem.* **2008**, *47*, 10378.
(4) Cooke, M. W.; Hanan, G. S. *Chem. Soc. Rev.* **2007**, *36*, 1466.
(5) Elvington, M.; Brown, J.; Arachchige, S. M.; Brewer, K. J. *J. Am. Chem. Soc.* **2007**, *129*, 10644.
(6) Fihri, A.; Artero, V.; Pereira, A.; Fontecave, M. *Dalton Trans.* **2008**, 5567.
(7) Gust, D.; Moore, T. A.; Moore, A. L. *Acc. Chem. Res.* **2001**, *34*, 40.
(8) Wasielewski, M. R. *Chem. Rev.* **1992**, *92*, 435.
(9) Aubert, V.; Guerchais, V.; Ishow, E.; Hoang-Thi, K.; Ledoux, I.; Nakatani, K.; Le Bozec, H. *Angew. Chem., Int. Ed.* **2008**, *47*, 577.
(10) Balzani, V.; Juris, A.; Venturi, M.; Campagna, S.; Serroni, S. *Chem. Rev.* **1996**, *96*, 759.
(11) Balzani, V.; Scandola, F. *Supramolecular Photochemistry*; Horwood: Chichester, U.K., 1991.
(12) Brown, W. R.; O'Boyle, N. M.; McGarvey, J. J.; Vos, J. G. *Chem. Soc. Rev.* **2005**, *34*, 641.
(13) Balzani, V.; Ceroni, P.; Juris, A.; Venturi, M.; Campagna, S.; Puntoriero, F.; Serroni, S. *Coord. Chem. Rev.* **2001**, *219*, 545.
(14) Welter, S.; Lafolet, F.; Cecchetto, E.; Vergeer, F.; De Cola, L. *ChemPhysChem* **2005**, *6*, 2417.
(15) Fleming, C. A.; Maxwell, K. A.; DeSimone, J. M.; Meyer, T. J.; Papanikolas, J. M. *J. Am. Chem. Soc.* **2001**, *123*, 10336.
(16) Baranoff, E.; Barigelletti, F.; Bonnet, S.; Collin, J. P.; Flamigni, L.; Mobian, P.; Sauvage, J. P. In *Photofunctional Transition Metal Complexes*; Springer-Verlag: Berlin, 2007; Vol. 123, pp 41−78.
(17) Blan, Z. Y.; Sumi, K.; Furue, M.; Sato, S.; Koike, K.; Ishitani, O. *Inorg. Chem.* **2008**, *47*, 10801.
(18) Walther, M. E.; Wenger, O. S. *Dalton Trans.* **2008**, 6311.
(19) Pelleteret, D.; Fletcher, N. C. *Eur. J. Inorg. Chem.* **2008**, 3597.
(20) Ventura, B.; Barbieri, A.; Barigelletti, F.; Seneclauze, J. B.; Retailleau, P.; Ziessel, R. *Inorg. Chem.* **2008**, *47*, 7048.
(21) Easun, T. L.; Alsindi, W. Z.; Towrie, M.; Ronayne, K. L.; Sun, X. Z.; Ward, M. D.; George, M. W. *Inorg. Chem.* **2008**, *47*, 5071.
(22) Otsuki, J.; Imai, A.; Sato, K.; Li, D. M.; Hosoda, M.; Owa, M.; Akasaka, T.; Yoshikawa, I.; Araki, K.; Suenobu, T.; Fukuzumi, S. *Chem.—Eur. J.* **2008**, *14*, 2709.
(23) Larsen, J.; Puntoriero, F.; Pascher, T.; McClenaghan, N.; Campagna, S.; Åkesson, E.; Sundström, V. *ChemPhysChem* **2007**, *8*, 2643.
(24) Goeb, S.; De Nicola, A.; Ziessel, R.; Sabatini, C.; Barbieri, A.; Barigelletti, F. *Inorg. Chem.* **2006**, *45*, 1173.

10.1021/ja907303t

quantitatively established through a detailed metrical analysis of the relative orientations of the donor/acceptor transition dipoles. Energy transfer rate constants on the order of 10^9 s^{-1} were observed in this system, driven in part by the charge-transfer nature of the optical transitions involved. It occurred to us that this basic compositional motif could provide a convenient platform for examining additional fundamental aspects of dipolar energy transfer. The notion of coupling to weakly absorbing acceptors was of particular interest in light of other work we have carried out on energy transfer involving spin-coupled di-iron(III) complexes.[42,43] Ligand-field states are intriguing candidates in this regard, due to their low oscillator strengths ($\varepsilon \sim 10-100$ M^{-1} cm^{-1}) while at the same time representing nearly ideal manifestations of the point-dipole approximation central to Förster theory.

Low-energy ligand-field states of first-row transition metal complexes have been implicated as energy acceptors in a number of studies.[44–58] For example, Ford and co-workers have shown that ligand-field states of Cr^{III} in *trans*-$Cr(cyclam)X_2^+$ ($X = Cl^-$ or ONO^-) complexes quench the photoluminescence of CdSe/ZnS core/shell quantum dots (QDs) via a Förster energy transfer mechanism.[59,60] The investigation showed that highly absorbing QDs act as antennae, which in turn photosensitize the weakly absorbing Cr^{III}-based $^4T_{1,2}$ ligand-field states of an attached $Cr(cyclam)(ONO)_2^+$ complex to trigger the release of NO; potential applications of this water-soluble system include the delivery of bioactive agents to specific physiological targets. Other recent examples of metal-centered acceptor states come from studies by Ward and co-workers, who have demonstrated significant quenching of MLCT-type emission by f−f acceptor states in Ln(III)-containing donor/acceptor systems.[61–65] The shielding of the 4f electron shell of the Ln(III) ions by the outer-core 5s and 5d electrons allows lanthanide coordination complexes to retain atomic-like absorption and emission profiles,[66] resulting in well-resolved spectra that allow for straightforward assignments of acceptor states that energetically overlap with the ^{3}MLCT emission profiles.

The clear-cut assignment of dipolar coupling in the $FeRe_3$ series mentioned above led us to design structurally analogous complexes that contain ligand-field states possessing favorable spectral overlap with the Re^I-based ^{3}MLCT emission spectra. In this report we describe the synthesis, structure, and photophysical properties of a series of molecules having the general formula $[Cu(pyacac)_2(Re(bpy')(CO)_3)_2](OTf)_2$. In these assemblies, the Cu^{II} metal centers are covalently attached to two *fac*-$Re(bpy')(CO)_3$ moieties through pyridyl-acetylacetonate bridging ligands (Scheme 1); variations in the substituents on the bipyridyl groups allowed for systematic energetic tuning of the emission profile of the Re^I-based ^{3}MLCT state relative to the absorption spectrum of the Cu^{II} center. Emissions from the Re^I fluorophores were all significantly attenuated relative to their $BeRe_2$ analogues, indicative of a reaction between the ^{3}MLCT excited state of the Re^I-bpy′ group and the central Cu^{II} ion. The confluence of data acquired on this system unequivocally establishes dipolar energy transfer as the dominant quenching mechanism. Moreover, the unique electronic properties of the Cu^{II} acceptor have allowed us to identify an absorption-specific pathway for energy transfer, a result that

(25) Shih, C.; Museth, A. K.; Abrahamsson, M.; Blanco-Rodriguez, A. M.; Di Bilio, A. J.; Sudhamsu, J.; Crane, B. R.; Ronayne, K. L.; Towrie, M.; Vlček, A.; Richards, J. H.; Winkler, J. R.; Gray, H. B. *Science* **2008**, *320*, 1760.
(26) Abrahamsson, M.; Jäger, M.; Kumar, R. J.; Österman, T.; Persson, P.; Becker, H. C.; Johansson, O.; Hammarström, L. *J. Am. Chem. Soc.* **2008**, *130*, 15533.
(27) Fleming, C. N.; Brennaman, M. K.; Papanikolas, J. M.; Meyer, T. J. *Dalton Trans.* **2009**, 3903.
(28) Meylemans, H. A.; Lei, C. F.; Damrauer, N. H. *Inorg. Chem.* **2008**, *47*, 4060.
(29) Fan, Y.; Zhang, L. Y.; Dai, F. R.; Shi, L. X.; Chen, Z. N. *Inorg. Chem.* **2008**, *47*, 2811.
(30) Wenger, O. S. *Coord. Chem. Rev.* **2009**, *253*, 1439.
(31) Benniston, A. C.; Harriman, A.; Li, P.; Patel, P. V.; Sams, C. A. *Chem.—Eur. J.* **2008**, *14*, 1710.
(32) Yamamoto, Y.; Sawa, S.; Funada, Y.; Morimoto, T.; Falkenstrom, M.; Miyasaka, H.; Shishido, S.; Ozeki, T.; Koike, K.; Ishitani, O. *J. Am. Chem. Soc.* **2008**, *130*, 14659.
(33) Bian, Z. Y.; Sumi, K.; Furue, M.; Sato, S.; Koike, K.; Ishitani, O. *Dalton Trans.* **2009**, 983.
(34) Alstrum-Acevedo, J. H.; Brennaman, M. K.; Meyer, T. J. *Inorg. Chem.* **2005**, *44*, 6802.
(35) Flamigni, L.; Collin, J. P.; Sauvage, J. P. *Acc. Chem. Res.* **2008**, *41*, 857.
(36) Balzani, V.; Credi, A.; Venturi, M. *ChemSusChem* **2008**, *1*, 26.
(37) Concepcion, J. J.; Jurss, J. W.; Templeton, J. L.; Meyer, T. J. *J. Am. Chem. Soc.* **2008**, *130*, 16462.
(38) Liu, F.; Concepcion, J. J.; Jurss, J. W.; Cardolaccia, T.; Templeton, J. L.; Meyer, T. J. *Inorg. Chem.* **2008**, *47*, 1727.
(39) Xu, Y. H.; Åkermark, T.; Gyollai, V.; Zou, D. P.; Eriksson, L.; Duan, L. L.; Zhang, R.; Åkermark, B.; Sun, L. C. *Inorg. Chem.* **2009**, *48*, 2717.
(40) Youngblood, W. J.; Lee, S. H. A.; Kobayashi, Y.; Hernandez-Pagan, E. A.; Hoertz, P. G.; Moore, T. A.; Moore, A. L.; Gust, D.; Mallouk, T. E. *J. Am. Chem. Soc.* **2009**, *131*, 926.
(41) Knight, T. E.; Guo, D.; Claude, J. P.; McCusker, J. K. *Inorg. Chem.* **2008**, *47*, 7249.
(42) Picraux, L. B.; Smeigh, A. L.; Guo, D.; McCusker, J. K. *Inorg. Chem.* **2005**, *44*, 7846.
(43) Picraux, L. B.; Weldon, B. T.; McCusker, J. K. *Inorg. Chem.* **2003**, *42*, 273.
(44) Benniston, A. C.; Harriman, A.; Li, P.; Sams, C. A. *J. Am. Chem. Soc.* **2005**, *127*, 2553.
(45) Weldon, F.; Hammarström, L.; Mukhtar, E.; Hage, R.; Gunneweg, E.; Hassnoot, J. G.; Reedijk, J.; Browne, W. R.; Guckian, A. L.; Vos, J. G. *Inorg. Chem.* **2004**, *43*, 4471.
(46) Bignozzi, C. A.; Bortolini, O.; Chiorboli, C.; Indelli, M. T.; Rampi, M. A.; Scandola, F. *Inorg. Chem.* **1992**, *31*, 172.
(47) Tamilarasan, R.; Endicott, J. F. *J. Phys. Chem.* **1986**, *90*, 1027.
(48) Kanemaguire, N. A. P.; Allen, M. M.; Vaught, J. M.; Hallock, J. S.; Heatherington, A. L. *Inorg. Chem.* **1983**, *22*, 3851.
(49) Lei, Y. B.; Buranda, T.; Endicott, J. F. *J. Am. Chem. Soc.* **1990**, *112*, 8820.
(50) Langford, V. S.; von Arx, M. E.; Hauser, A. *J. Phys. Chem. A* **1999**, *103*, 7161.
(51) Wolcan, E.; Alessandrini, J. L.; Feliz, M. R. *J. Phys. Chem. B* **2005**, *109*, 22890.
(52) Neuman, D.; Ostrowski, A. D.; Mikhailovsky, A. A.; Absalonson, R. O.; Strouse, G. F.; Ford, P. C. *J. Am. Chem. Soc.* **2008**, *130*, 168.
(53) Otsuka, T.; Sekine, A.; Fujigasaki, N.; Ohashi, Y.; Kaizu, Y. *Inorg. Chem.* **2001**, *40*, 3406.
(54) Albinsson, B.; Mårtensson, J. *J. Photochem. Photobiol. C: Photochem. Rev.* **2008**, *9*, 138.
(55) Ward, M. D.; McCleverty, J. A. *Dalton Trans.* **2002**, 275.
(56) Laye, R. H.; Couchman, S. M.; Ward, M. D. *Inorg. Chem.* **2001**, *40*, 4089.
(57) Scandola, F.; Indelli, M. T.; Chiorboli, C.; Bignozzi, C. A. *Top. Curr. Chem.* **1990**, *158*, 73.
(58) Scandola, F.; Bignozzi, C. A.; Chiorboli, C.; Indelli, M. T.; Rampi, M. A. *Coord. Chem. Rev.* **1990**, *97*, 299.
(59) Neuman, D.; Ostrowski, A. D.; Mikhailovsky, A. A.; Absalonson, R. O.; Strouse, G. F.; Ford, P. C. *J. Am. Chem. Soc.* **2008**, *130*, 168.
(60) Ford, P. C. *Acc. Chem. Res.* **2008**, *41*, 190.
(61) Shavaleev, N. M.; Accorsi, G.; Virgili, D.; Bell, D. R.; Lazarides, T.; Calogero, G.; Armaroli, N.; Ward, M. D. *Inorg. Chem.* **2005**, *44*, 61.
(62) Davies, G. M.; Pope, S. J. A.; Adams, H.; Faulkner, S.; Ward, M. D. *Inorg. Chem.* **2005**, *44*, 4656.
(63) Kennedy, F.; Shavaleev, N. M.; Koullourou, T.; Bell, Z. R.; Jeffery, J. C.; Faulkner, S.; Ward, M. D. *Dalton Trans.* **2007**, 1492.
(64) Baca, S. G.; Adams, H.; Sykes, D.; Faulkner, S.; Ward, M. D. *Dalton Trans.* **2007**, 2419.
(65) Baca, S. G.; Pope, S. J. A.; Adams, H.; Ward, M. D. *Inorg. Chem.* **2008**, *47*, 3736.
(66) Buono-Core, G. E.; Li, H. *Coord. Chem. Rev.* **1990**, *99*, 55.

Scheme 1

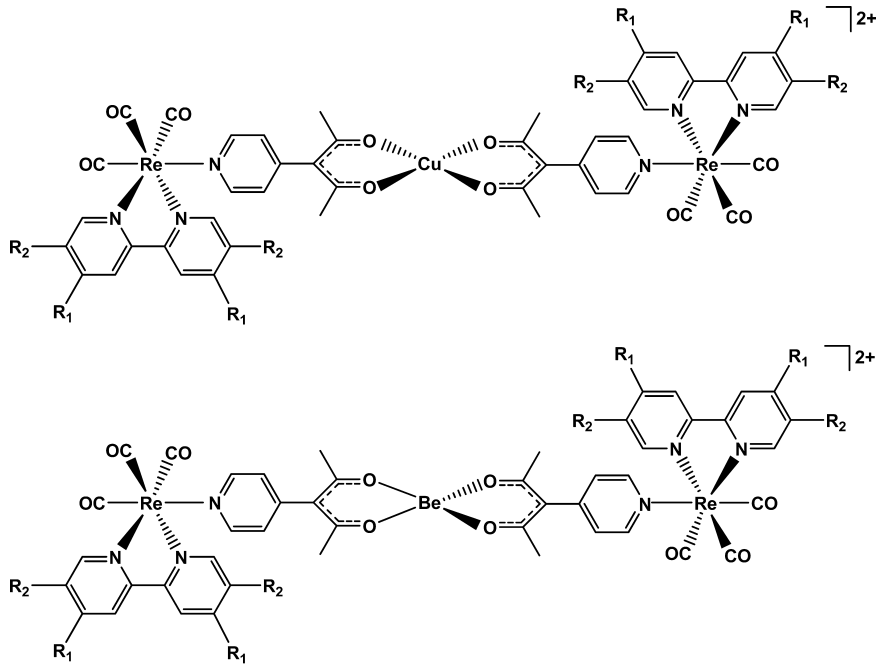

1 (Cu) and **6** (Be): $R_1 = R_2 = CH_3$ **2** (Cu) and **7** (Be): $R_1 = CH_3$, $R_2 = H$
3 (Cu) and **8** (Be): $R_1 = R_2 = H$ **4** (Cu) and **9** (Be): $R_1 = Cl$, $R_2 = H$
5 (Cu) and **10** (Be): $R_1 = CO_2Et$, $R_2 = H$

illustrates the role of relative transition dipole orientation operating at the atomic-orbital level.

Experimental Section

General Procedures. All solvents used were purified and dried according to previously reported methods.[67] Spectroscopic grade CH_2Cl_2 was used for all photophysical measurements and was dried under CaH_2 reflux until no water was detected by ^1H NMR. Solvents for both steady-state and time-resolved emission measurements were thoroughly degassed using freeze−pump−thaw techniques. 3-(4-pyridyl)-2,4-pentanedione,[68] Cu(pyacac)$_2$,[69] Cu(phacac)$_2$,[70] Be(pyacac)$_2$,[71] Re(tmb)(CO)$_3$(OTf) (where tmb = 4,4′-5,5′-tetramethyl-2,2′-bipyridine),[72] Re(dmb)(CO)$_3$(OTf) (where dmb = 4,4′-dimethyl-2,2′-bipyridine),[72] Re(bpy)(CO)$_3$(OTf) (where bpy = 2,2′-bipyridine),[72] Re(dclb)(CO)$_3$(OTf) (where dclb = 4,4′-dichloro-2,2′-bipyridine),[72] Re(deeb)(CO)$_3$(OTf) (where deeb = 4,4′-diethylester-2,2′-bipyridine),[72] and *fac*-[Re(bpy)(CO)$_3$(4-Etpy)](PF$_6$)[73] (4-Etpy = 4-ethylpyridine) were prepared according to literature procedures. 3-phenyl-2,4-pentanedione was purchased from TCI America. Elemental analyses and FT-IR data were obtained through the analytical facilities at Michigan State University; mass spectra were obtained through the analytical facilities at The University of South Carolina.

General Procedure for CuRe$_2$ Complexes (1−5). In a typical experiment, Cu(pyacac)$_2$ (0.2 mmol) and Re(bpy′)(CO)$_3$(OTf) (0.4 mmol) were dissolved in 40 mL of hot THF, and the solution was purged with argon for 20 min. The reaction mixture was then fit with a condenser and stirred under argon for 24 h in the dark, after which time a precipitate corresponding to the desired product was formed. The green-colored solids were collected, washed with dry THF, and recrystallized multiple times from acetonitrile/ether (1:1) or CH_2Cl_2/hexanes (1:1).

[Cu(pyacac)$_2$(Re(tmb)(CO)$_3$)$_2$](OTf)$_2$ (1). Amounts of 99 mg (0.24 mmol) of Cu(pyacac)$_2$ and 300 mg (0.475 mmol) of Re(tmb)(CO)$_3$(OTf) were used in the preparation of compound **1**. Yield: 129 mg (32%). Anal. Calcd for $C_{56}H_{52}N_6F_6O_{16}S_2CuRe_2$: C, 40.06; H, 3.12; N, 5.00. Found: C, 40.19; H, 3.30; N, 4.79. IR (KBr, cm^{-1}): 2030 s, 1925 s, 1902 s, 1614 m, 1575 s, 1417 m, 1261 m, 1157 m, 1032 s, 639 m. MS [ESI$^+$, *m*/*z* (rel int)]: 690.5 (62) {[Cu(pyacac)$_2$(Re(tmb)(CO)$_3$)$_2$]}$^{2+}$, 1530.1 (2) {[Cu(pyacac)$_2$-(Re(tmb)(CO)$_3$)$_2$](OTf)}$^+$.

[Cu(pyacac)$_2$(Re(dmb)(CO)$_3$)$_2$](OTf)$_2$ (2). Amounts of 77 mg (0.19 mmol) of Cu(pyacac)$_2$ and 219 mg (0.369 mmol) of Re(dmb)(CO)$_3$(OTf) were used in the preparation of compound **2**. Yield: 132 mg (44%). Anal. Calcd for $C_{52}H_{44}N_6F_6O_{16}S_2CuRe_2$: C, 38.48; H, 2.73; N, 5.18. Found: C, 38.22; H, 2.75; N, 5.27. IR (KBr, cm^{-1}): 2030 s, 1927 s, 1915 s, 1619 m, 1573 s, 1419 m, 1259 m, 1159 m, 1031 m, 638 m. MS [ESI$^+$, *m*/*z* (rel int)]: 662.4 (60) {[Cu(pyacac)$_2$(Re(dmb)(CO)$_3$)$_2$]}$^{2+}$, 1474 (4) {[Cu(pyacac)$_2$-(Re(dmb)(CO)$_3$)$_2$](OTf)}$^+$.

[Cu(pyacac)$_2$(Re(bpy)(CO)$_3$)$_2$](OTf)$_2$ (3). Quantities of 80 mg (0.19 mmol) of Cu(pyacac)$_2$ and 220 mg (0.382 mmol) of Re(bpy)(CO)$_3$(OTf) were used in the preparation of compound **3**. X-ray quality crystals were obtained by slow diffusion of ether into an acetonitrile solution of the compound. Yield: 255 mg (65%). Anal. Calcd for $C_{48}H_{36}N_6F_6O_{16}S_2CuRe_2$: C, 36.79; H, 2.32; N, 5.36. Found: C, 36.94; H, 2.43; N, 5.25. IR (KBr, cm^{-1}): 2033 s, 1913 s, 1604 w, 1575 s, 1419 m, 1259 m, 1160 m, 1031 m, 772 m, 638 m. MS [ESI$^+$, *m*/*z* (rel int)]: 634.4 (100) {[Cu(pyacac)$_2$(Re(bpy)-(CO)$_3$)$_2$]}$^{2+}$, 1417.8 (5) {[Cu(pyacac)$_2$(Re(bpy)(CO)$_3$)$_2$](OTf)}$^+$.

[Cu(pyacac)$_2$(Re(dclb)(CO)$_3$)$_2$](OTf)$_2$ (4). Amounts of 73 mg (0.18 mmol) of Cu(pyacac)$_2$ and 227 mg (0.352 mmol) of

(67) Perrin, D. D.; Armarego, W. L. F. *Purification of Laboratory Chemicals*, 3rd ed.; Pergamon Press: Oxford, U.K., 1988.
(68) Mackay, L. G.; Anderson, H. L.; Sanders, J. K. M. *J. Chem. Soc., Perkin Trans. 1* **1995**, *18*, 2269.
(69) Chen, B.; Fronczek, F. R.; Maverick, A. W. *Chem. Commun.* **2003**, 2166.
(70) Carmichael, J. W., Jr.; Steinrauf, L. K.; Belford, R. L. *J. Chem. Phys.* **1965**, *43*, 3959.
(71) Vreshch, V. D.; Chernega, A. N.; Howard, J. A. K.; Sieler, J.; Domasevitch, K. V. *Dalton Trans.* **2003**, 1707.
(72) Hino, J. K.; Della Ciana, L.; Dressick, W. J.; Sullivan, B. P. *Inorg. Chem.* **1992**, *31*, 1072.
(73) Caspar, J. V.; Meyer, T. J. *J. Phys. Chem.* **1983**, *87*, 952.

$Re(dclb)(CO)_3(OTf)$ were used in the preparation of compound **4**. Yield: 195 mg (65%). Anal. Calcd for $C_{48}H_{32}N_6Cl_4F_6O_{16}S_2CuRe_2$: C, 33.82; H, 1.89; N, 4.93. Found: C, 33.69; H, 1.99; N, 4.61. IR (KBr, cm^{-1}): 2033 s, 1933 s, 1574 s, 1468 m, 1257 m, 1156 m, 1031 m, 840 w, 638 m. MS [ESI^+, *m/z* (rel int)]: 703.3 (30) $\{[Cu(pyacac)_2(Re(dclb)(CO)_3)_2]\}^{2+}$, 1555.6 (1) $\{[Cu(pyacac)_2(Re(dclb)(CO)_3)_2](OTf)\}^+$.

$[Cu(pyacac)_2(Re(deeb)(CO)_3)_2](OTf)_2$ (5). Quantities of 74 mg (0.18 mmol) of $Cu(pyacac)_2$ and 255 mg (0.354 mmol) of $Re(deeb)(CO)_3(OTf)$ were used in the preparation of compound **5**. Yield: 200 mg (61%). Anal. Calcd for $C_{60}H_{52}N_6F_6O_{24}S_2CuRe_2 \cdot CH_2Cl_2$: C, 38.15; H, 2.79; N, 4.30. Found: C, 37.90; H, 2.62; N, 4.66. IR (KBr, cm^{-1}): 2035 s, 1926 s, 1732 m, 1573 m, 1408 m, 1323 m, 1263 s, 1154 m, 1031 m, 767 m, 638 m. MS [ESI^+, *m/z* (rel int)]: 778.5 (100) $\{[Cu(pyacac)_2(Re(deeb)(CO)_3)_2]\}^{2+}$, 1706.1 (3) $\{[Cu(pyacac)_2(Re(deeb)(CO)_3)_2](OTf)\}^+$.

General Procedure for $BeRe_2$ Complexes (6−10). These compounds were prepared analogously to complexes **1**−**5** by replacing $Cu(pyacac)_2$ with $Be(pyacac)_2$. The volumes of the reaction mixtures were reduced to ∼10 mL, and hexanes were slowly added to precipitate the $[Be(pyacac)_2(Re(bpy')(CO)_3)_2](OTf)_2$ compounds. The resulting yellow-colored solids were collected, washed with dry THF, and recrystallized multiple times from acetonitrile/ether (1:1).

$[Be(pyacac)_2(Re(tmb)(CO)_3)_2](OTf)_2$ (6). Amounts of 67 mg (0.19 mmol) of $Be(pyacac)_2$ and 233 mg (0.369 mmol) of $Re(tmb)(CO)_3(OTf)$ were used in the preparation of compound **6**. X-ray quality crystals were obtained by slow diffusion of ether into an acetonitrile solution of the compound. Yield: 135 mg (45%). Anal. Calcd for $C_{56}H_{52}N_6F_6O_{16}S_2BeRe_2$: C, 41.40; H, 3.23; N, 5.17. Found: C, 41.53; H, 3.44; N, 5.00. IR (KBr, cm^{-1}): 2031 s, 1916 s, 1613 m, 1575 m, 1417 m, 1261 m, 1155 m, 1031 m, 847 m, 638 m. MS [ESI^+, *m/z* (rel int)]: 663.2 (86) $\{[Be(pyacac)_2(Re(tmb)(CO)_3)_2]\}^{2+}$, 1475.5 (2) $\{[Be(pyacac)_2(Re(tmb)(CO)_3)_2](OTf)\}^+$.

$[Be(pyacac)_2(Re(dmb)(CO)_3)_2](OTf)_2$ (7). Amounts of 70 mg (0.20 mmol) of $Be(pyacac)_2$ and 231 mg (0.390 mmol) of $Re(dmb)(CO)_3(OTf)$ were used in the preparation of compound **7**. Yield: 124 mg (41%). Anal. Calcd for $C_{52}H_{44}N_6F_6O_{16}S_2BeRe_2$: C, 39.82; H, 2.83; N, 5.36. Found: C, 40.00; H, 2.94; N, 5.47. IR (KBr, cm^{-1}): 2031 s, 1915 s, 1620 m, 1576 s, 1418 m, 1260 m, 1159 m, 1031 s, 847 m, 638 m. MS [ESI^+, *m/z* (rel int)]: 635.2 (100) $\{[Be(pyacac)_2(Re(dmb)(CO)_3)_2]\}^{2+}$, 1419.4 (2) $\{[Be(pyacac)_2(Re(dmb)(CO)_3)_2](OTf)\}^+$.

$[Be(pyacac)_2(Re(bpy)(CO)_3)_2](OTf)_2$ (8). Quantities of 72 mg (0.20 mmol) of $Be(pyacac)_2$ and 228 mg (0.397 mmol) of $Re(bpy)(CO)_3(OTf)$ were used in the preparation of compound **8**. After 24 h of stirring in hot THF, a yellow crystalline material formed. The reaction mixture was allowed to cool to room temperature, and the yellow material and solution were separated by filtration. ESI-MS and single-crystal X-ray data of the yellow crystalline material were used to identify this side-product as $[(Be_3(OH)_3(pyacac)_3)((Re(bpy)(CO)_3)_3)](OTf)_3$, whose structure is built upon a Be_3O_3 core that has been observed previously.[74–76] Details concerning the structure of this compound can be found elsewhere.[77]

The filtrate from the aforementioned separation was reduced to ∼10 mL, and hexanes were added to produce a yellow solid. The solid was collected, washed with dry THF, and recrystallized from acetonitrile/ether. Yield: 31 mg (10%). Anal. Calcd for $C_{48}H_{36}N_6F_6O_{16}S_2BeRe_2$: C, 38.12; H, 2.40; N, 5.56. Found: C, 38.25; H, 2.61; N, 5.39. IR (KBr, cm^{-1}): 2033 s, 1919 s, 1604 m, 1576 s, 1419 m, 1261 m, 1161 m, 1031 m, 849 m, 771 m, 636 m. MS [ESI^+, *m/z* (rel int)]: 607.1 (83) $\{[Be(pyacac)_2(Re(bpy)(CO)_3)_2]\}^{2+}$.

$[Be(pyacac)_2(Re(dclb)(CO)_3)_2](OTf)_2$ (9). Quantities of 66 mg (0.18 mmol) of $Be(pyacac)_2$ and 234 mg (0.364 mmol) of $Re(dclb)(CO)_3(OTf)$ were used in the preparation of compound **9**. Yield: 199 mg (66%). Anal. Calcd for $C_{48}H_{32}N_6Cl_4F_6O_{16}S_2BeRe_2$: C, 34.94; H, 1.95; N, 5.09. Found: C, 35.06; H, 2.22; N, 4.81. IR (KBr, cm^{-1}): 2035 s, 1919 s, 1575 s, 1467 m, 1258 s, 1158 m, 1030 m, 846 m, 755 w, 638 m. MS [ESI^+, *m/z* (rel int)]: 676.0 (100) $\{[Be(pyacac)_2(Re(dclb)(CO)_3)_2]\}^{2+}$, 1501.1 (1) $\{[Be(pyacac)_2(Re(dclb)(CO)_3)_2](OTf)\}^+$.

$[Be(pyacac)_2(Re(deeb)(CO)_3)_2](OTf)_2$ (10). Amounts of 60 mg (0.17 mmol) of $Be(pyacac)_2$ and 240 mg (0.334 mmol) of $Re(deeb)(CO)_3(OTf)$ were used in the preparation of compound **10**. Yield: 136 mg (45%). Anal. Calcd for $C_{60}H_{52}N_6F_6O_{24}S_2BeRe_2$: C, 40.02; H, 2.91; N, 4.67. Found: C, 39.63; H, 2.92; N, 4.45. IR (KBr, cm^{-1}): 2035 s, 1925 s, 1732 m, 1576 m, 1464 m, 1323 m, 1263 s, 1155 m, 1031 m, 849 m, 767 m, 638 m. MS [ESI^+, *m/z* (rel int)]: 751.3 (79) $\{[Be(pyacac)_2(Re(deeb)(CO)_3)_2]\}^{2+}$, 1651.6 (2) $\{[Be(pyacac)_2(Re(deeb)(CO)_3)_2](OTf)\}^+$.

Table 1. Crystallographic Data for $[Cu(pyacac)_2(Re(bpy)(CO)_3)_2](OTf)_2$ (**3**) and $[Be(pyacac)_2(Re(tmb)(CO)_3)_2](OTf)_2$ (**6**)

	3	**6**
formula	$C_{48}H_{36}N_6F_6O_{16}S_2CuRe_2$	$C_{56}H_{52}N_6F_6O_{16}S_2BeRe_2$
M_w	1566.9	1624.6
cryst syst	monoclinic	monoclinic
space group	*P*2(1)/*c*	*P*2(1)/*c*
T/K	173(2)	173(2)
a/Å	10.3213(12)	18.7639(3)
b/Å	24.532(3)	16.9382(3)
c/Å	12.1608(14)	21.0542(4)
α/deg	90	90
β/deg	104.027(2)	106.241(1)
γ/deg	90	90
V/Å^3	2987.3(6)	6424.5(2)
Z	2	4
D_c/g cm^{-3}	1.833	1.696
$2\theta_{max}$	50	136.4
reflns measd	29 110	72 385
indep reflns	5253	11 601
obsd reflns [$I > 2\sigma(I)$]	4827	10 856
μ(Mo Kα)/cm^{-1}	4.556	8.63
R_{int}	0.026	0.041
R1[a]	0.019	0.048
wR2[b]	0.0443	0.132
GOF	1.005	1.050

[a] $R1 = \sum||F_o| - |F_c||/\sum|F_o|$. [b] $wR2 = [\sum w(F_o^2 - F_c^2)^2/\sum w(F_o^2)^2]^{1/2}$, $w = 1/[\sigma^2(F_o^2) + (aP)^2 + bP]$, where $P = [F_o^2 + 2F_c^2]/3$.

Physical Measurements. X-ray Structure Determinations. Single-crystal X-ray diffraction data for complexes **3** and **6** were acquired at the X-ray facility of Michigan State University. Diffraction data were collected on a Siemens SMART diffractometer with graphite-monochromatic Mo Kα radiation ($\lambda = 0.71073$ Å). Data were collected at −100 °C by using an Oxford Cryosystems low-temperature device. Crystallographic data are summarized in Table 1; selected bond distances and angles are listed in Table 2. Lattice parameters were obtained from least-squares analyses, and data were integrated with the program SAINT.[78] The integration method employed a three-dimensional profiling algorithm, and all data were corrected for Lorentz and polarization factors, as well as for crystal decay effects. The absorption correction program SADABS[79] was employed to correct the data for absorption effects. The structures were solved by direct methods and expanded using Fourier techniques. All structure calculations were performed with

(74) Klein, R. M.; Bailar, J. C. *Inorg. Chem.* **1963**, *2*, 1187.
(75) Sohrin, Y.; Matsui, M.; Hata, Y.; Hasegawa, H.; Kokusen, H. *Inorg. Chem.* **1994**, *33*, 4376.
(76) Barbaro, P.; Cecconi, F.; Ghilardi, C. A.; Midollini, S.; Orlandini, A.; Alderighi, L.; Peters, D.; Vacca, A.; Chinea, E.; Mederos, A. *Inorg. Chim. Acta* **1997**, *262*, 187.
(77) Knight, T. E. Dipolar Energy Transfer in Rhenium(I) Polypyridyl-Based Donor-Acceptor Assemblies. Ph.D. Thesis, Michigan State University, 2009.
(78) *SAINT, ver 6.02a*; Bruker AXS, Inc.: Madison, WI, 2000.
(79) Sheldrick, G. M. *SADABS ver 2.03*; Bruker AXS, Inc.: Madison, WI, 2000.

Table 2. Selected Bond Distances and Angles for [Cu(pyacac)$_2$(Re(bpy)(CO)$_3$)$_2$](OTf)$_2$ (**3**) and [Be(pyacac)$_2$(Re(tmb)(CO)$_3$)$_2$](OTf)$_2$ (**6**)

3		**6**	
Bond Distances (Å)			
Cu(1)−O(1)	1.920(2)	Be(1)−O(1)	1.618(9)
Cu(1)−O(2)	1.914(2)	Be(1)−O(2)	1.590(9)
Cu(1)−O(1A)	1.920(2)	Be(1)−O(6)	1.601(9)
Cu(1)−O(2A)	1.914(2)	Be(1)−O(7)	1.610(10)
Re(1)−N(1)	2.168(2)	Re(1)−N(1)	2.220(5)
Re(1)−N(2)	2.170(2)	Re(1)−N(2)	2.156(6)
Re(1)−N(3)	2.214(2)	Re(1)−N(3)	2.161(5)
Re(1)−C(22)	1.918(4)	Re(1)−C(25)	1.921(7)
Re(1)−C(23)	1.927(4)	Re(1)−C(26)	1.922(7)
Re(1)−C(24)	1.915(4)	Re(1)−C(27)	1.913(7)
Cu(1)−O(8)	2.702		
Cu(1)−O(8A)	2.545		
Cu(1)···Re(1)	9.707	Be(1)···Re(1)	9.466
Cu(1)···Re(1A)	9.707	Be(1)···Re(2)	9.416
Bond Angles (deg)			
O(1)−Cu(1)−O(2)	92.0(8)	O(1)−Be(1)−O(2)	105.6(5)
O(1)−Cu(1)−O(1A)	180.0(13)	O(1)−Be(1)−O(6)	108.8(6)
N(1)−Re(1)−N(2)	75.02(9)	N(2)−Re(1)−N(3)	75.3(2)
C(22)−Re(1)−N(3)	95.22(11)	C(26)−Re(1)−N(1)	92.0(2)
C(23)−Re(1)−N(3)	175.8(5)	C(25)−Re(1)−N(1)	176.9(3)
plane 1···plane 2[a]	87.414	plane 1···plane 2[c]	60.448
plane 1···plane 2[b]	87.414	plane 1···plane 2[d]	75.75

[a] Plane 1 is defined by atoms O(1), O(2), C(1), C(2), C(3), C(4), C(5); plane 2 is defined by atoms N(3), C(6), C(7), C(8), C(9), C(10). [b] Given by the atoms that define the two planes in the adjacent pyacac ligand. [c] Plane 1 is defined by atoms O(1), O(2), C(1), C(2), C(3), C(4), C(5); plane 2 is defined by atoms N(1), C(6), C(7), C(8), C(9), C(10). [d] Given by the atoms that define the two planes in the adjacent pyacac ligand.

the SHELXTL 6.12 software package.[80] Anisotropic thermal parameters were refined for all non-hydrogen atoms. Hydrogen atoms were localized in their calculation positions and refined by using the riding model. Further details concerning the structure determinations may be found in the Supporting Information.

Cyclic Voltammetry. Electrochemical measurements were carried out in a Ar-filled drybox (Vacuum Atmospheres) using a BAS CV-50W electrochemical analyzer. A standard three-electrode arrangement was utilized consisting of a Pt working electrode, graphite counter electrode, and a Ag/$AgNO_3$ reference electrode. Measurements were carried out in CH_3CN solution that was 0.1 M in NBu_4PF_6. Potentials are reported versus the ferrocene/ferrocenium couple, which was used as an internal standard.

Electronic Absorption and Steady-State Emission Spectroscopies. Extinction coefficients for all compounds were acquired in room-temperature CH_2Cl_2 solution using a Varian Cary 50 UV−visible spectrophotometer. Steady-state emission spectra were acquired using a Spex Fluoromax fluorimeter and corrected for instrumental response using a NIST standard of spectral irradiance (Optronic Laboratories, Inc., OL220 M tungsten quartz lamp).[81] Spectra were acquired on samples dissolved in thoroughly degassed CH_2Cl_2 under optically dilute conditions (o.d. ∼0.1) and sealed under an argon atmosphere in 1 cm path length quartz cuvettes.

Radiative quantum yields (Φ_r) for complexes **6**−**10** were determined relative to *fac*-[Re(bpy)(CO)$_3$(4-Etpy)](PF$_6$) ($\Phi_r = 0.18$ in CH_2Cl_2).[73] Quantum yields were calculated according to eq 1,

$$\Phi_{unk} = \Phi_{std}\frac{(I_{unk}/A_{unk})}{(I_{std}/A_{std})}\left(\frac{\eta_{unk}}{\eta_{std}}\right)^2 \quad (1)$$

where Φ_{unk} and Φ_{std} are the radiative quantum yields of the sample and the standard, respectively, I_{unk} and I_{std} represent the areas of the corrected emission profiles for the sample and the standard, A_{unk} and A_{std} are the absorbance values of the sample and the standard at the excitation wavelength, and η_{unk} and η_{std} correspond to the indices of refraction of the sample and standard solutions (taken to be equal to the neat solvents). Excitation wavelengths were 355 nm for the tmb, dmb, and bpy analogues, 375 nm for the dclb analogue, and 400 nm for the deeb analogue. The corrected excitation spectrum of *fac*-[Re(bpy)(CO)$_3$(4-Etpy)](PF$_6$) in CH_2Cl_2 compared favorably with the compound's absorption spectrum over the range of wavelengths examined (355−400 nm), implying that the radiative quantum yield for *fac*-[Re(bpy)(CO)$_3$(4-Etpy)](PF$_6$) does not vary significantly over this spectral window; the reported value of $\Phi_r = 0.18$ was therefore used for determining the radiative quantum yields at $\lambda_{ex} = 355$, 375, and 400 nm. Values for the zero-point energy gap (E_{00}) of the Re^I-based ^{3}MLCT excited states were determined by fitting emission profiles based on the approach described by Claude and Meyer.[82] Wavelength data were converted to energy units employing the correction of Parker and Rees;[83] the best fit was determined by visual inspection of the results of a least-squares minimization routine.

Time-Resolved Emission Spectroscopy. Nanosecond time-resolved emission data for the $BeRe_2$ model complexes **6**−**10** were collected using a Nd:YAG-based laser spectrometer that has been described previously.[81] Data were acquired at room temperature in thoroughly degassed CH_2Cl_2 solutions having absorbances of ∼0.1 at the excitation wavelengths. Samples were sealed under an argon atmosphere in 1 cm path length quartz cuvettes. The decay traces correspond to an average of 250 shots of the signal probed at the emission maximum of each compound.

Picosecond time-resolved emission data for the $CuRe_2$ complexes **1**−**5** were collected using a time-correlated single-photon counting (TCSPC) apparatus that has been described previously.[84] Data were acquired in thoroughly degassed CH_2Cl_2 solutions having absorbances of ∼0.1 at the excitation wavelength. Samples were sealed under an argon atmosphere in 1 cm path length quartz cuvettes. Each reported decay trace corresponds to a signal average of six data sets, with each data set resulting from ca. 30 min of data acquisition time. The decay traces for all five complexes manifest a small baseline offset within the data acquisition window due to the presence of a small amount of an emissive impurity that was identified as *fac*-[Re(bpy′)(CO)$_3$(pyacac)] on the basis of their similarities to the long-lived kinetics observed for the corresponding $BeRe_2$ model complexes. Decay traces for all five Cu-containing complexes were therefore fit with biexponential kinetic models by fixing the long-lived component to the lifetime of the corresponding $BeRe_2$ complex. Data were fit using the OriginPro 7.5 software package.[85]

DFT Calculations. The Gaussian 03[86] software package was used for all calculations. The nuclear coordinates used for Cu(phacac)$_2$ in the calculations were based on the single-crystal X-ray structure reported by Carmichael et al.[70] The geometry optimization was performed with the UB3LYP functional and LANL2DZ basis set. The effect of CH_2Cl_2 solvent on the optimization was modeled using the polarizable continuum model (PCM);[87−90] no symmetry restrictions were imposed. Time-

(80) Sheldrick, G. M. *SHELXTL ver 6.12*; Bruker AXS, Inc.: Madison, WI, 2001.
(81) Damrauer, N. H.; Boussie, T. R.; Devenney, M.; McCusker, J. K. *J. Am. Chem. Soc.* **1997**, *119*, 8253.
(82) Claude, J. P.; Meyer, T. J. *J. Phys. Chem.* **1995**, *99*, 51.
(83) Parker, C. A.; Rees, W. T. *Analyst (London)* **1960**, *85*, 587.
(84) DeWitt, L.; Blanchard, G. J.; LeGoff, E.; Benz, M. E.; Liao, J. H.; Kanatzidis, M. G. *J. Am. Chem. Soc.* **1993**, *115*, 12158.
(85) *Origin, 7.5 ed*; OriginLab Corp: Northhampton, MA, 1991−2004,
(86) Frisch, M. J.; et al. *Gaussian 03*; Gaussian, Inc.: Wallingford, CT, 2004.
(87) Miertuš, S.; Scrocco, S.; Tomasi, J. *Chem. Phys.* **1981**, *55*, 117.

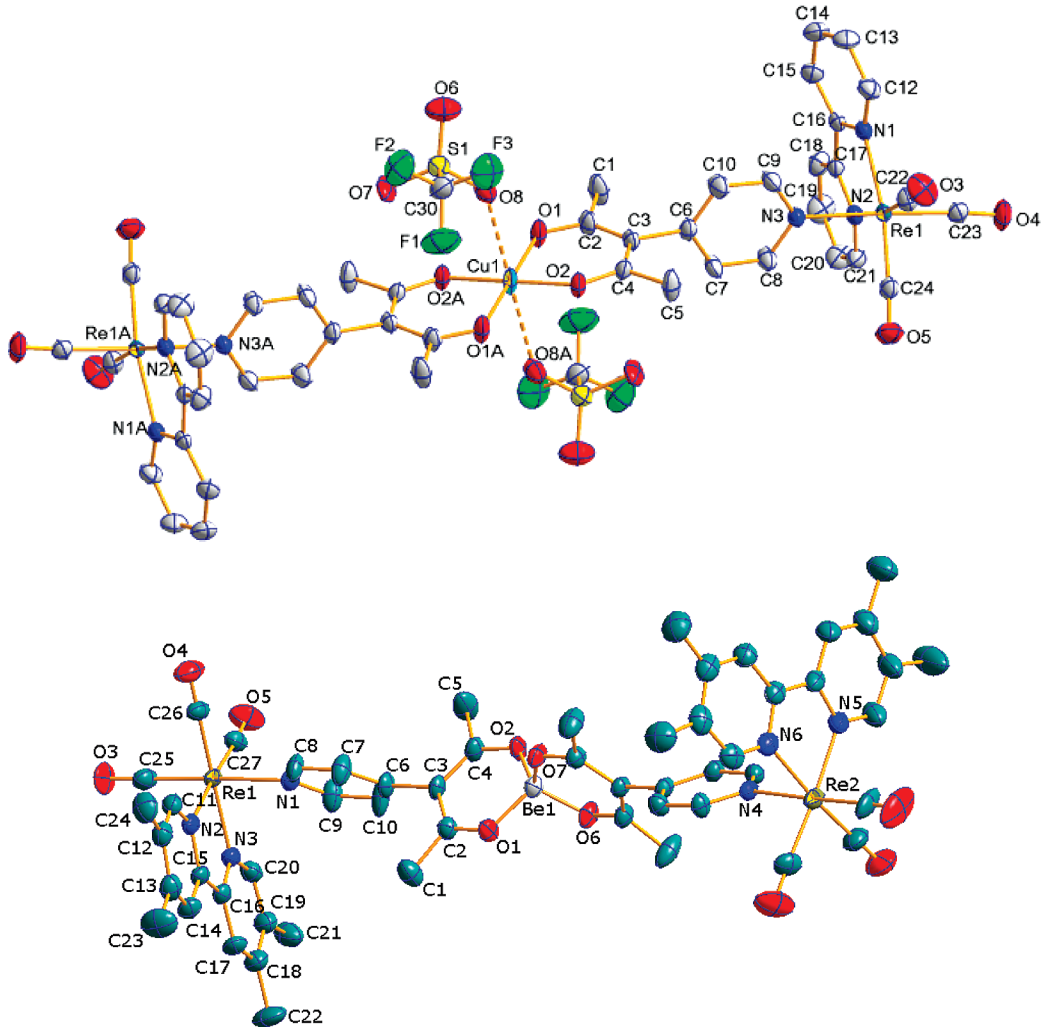

Figure 1. Drawings of $[Cu(pyacac)_2(Re(bpy)(CO)_3)_2](OTf)_2$ (**3**, top) and the cation of $[Be(pyacac)_2(Re(tmb)(CO)_3)_2](OTf)_2$ (**6**, bottom) obtained from single-crystal X-ray structure determinations. Atoms are represented as 50% probability thermal ellipsoids.

dependent density functional theory (TD-DFT) calculations were performed using the UB3LYP functional and the 6-311G** basis set; the influence of the CH_2Cl_2 solvent was accounted for using the PCM model. All calculations used tight convergence criteria[91] assuming a molecular charge of 0 and a ground-state spin of $S = 1/2$. The molecular orbitals were generated using GaussView.[92]

Results and Discussion

Synthesis and Structural Characterization. Our interest in developing these systems was to investigate dipole−dipole energy transfer processes in structurally well-defined assemblies that possess weakly absorbing acceptors. The choice of using Re^I and Cu^{II} was based on the well-known MLCT-based reactivity of Re^I and the low oscillator strengths of absorptions associated with Cu^{II} ligand-field states. The utilization of the $M(pyacac)_2$ core ($M = Cu^{II}$ and Be^{II}) as a ligand for $Re(bpy')(CO)_3(OTf)$ allowed the pyridyl group to displace the weakly coordinating triflate anion and generate the dicationic $CuRe_2$ and $BeRe_2$ complexes. The formation of the trinuclear assembly was facilitated by the low steric crowding afforded by the 180° separation of the two pyacac ligands, along with the propensity of both metal ions to form four-coordinate complexes.

The ESI-MS data for complexes **1**−**10** in acetonitrile solution are consistent with the formation of the $CuRe_2$ and $BeRe_2$ assemblies. For example, complex **3** shows peaks corresponding to $[Cu(pyacac)_2(Re(bpy)(CO)_3)_2]^{2+}$ and $[Cu(pyacac)_2(Re(bpy)(CO)_3)_2](OTf)^+$. X-ray quality crystals for complexes **3** and **6** were generated by diffusion of ether into an acetonitrile solution of the complexes over the course of approximately one week; this in turn provides additional evidence for the general robustness of complexes **1**−**10** in solution.

$[Cu(pyacac)_2(Re(bpy)(CO)_3)_2](OTf)_2$ (**3**) and $[Be(pyacac)_2(Re(tmb)(CO)_3)_2](OTf)_2$ (**6**) both crystallize in the monoclinic space group $P2(1)/c$. Crystallographic details are given in Table 1, with selected bond distances and angles for the two complexes listed in Table 2. The coordination environment about the central metal ion in complex **3** (Figure 1) is formed from the four oxygen atoms of the acac ligands. The Cu−O bond distances

(88) Tomasi, J.; Bonaccorsi, R.; Cammi, R.; Valle, F. J. *J. Mol. Struc. (THEOCHEM)* **1991**, *234*, 401.
(89) Tomasi, J.; Bonaccorsi, R. *Croat. Chem. Acta* **1992**, *65*, 29.
(90) Tomasi, J.; Persico, M. *Chem. Rev.* **1994**, *94*, 2027.
(91) Frisch, M. J.; Frisch, A. *Gaussian 98 User's Reference*; Gaussian, Inc.: Pittsburgh, 1998.
(92) Dennington, R., II; Keith, T.; Millam, J. *GaussView*, 4.1.2 ed.; Semichem, Inc.: Shawnee Mission, KS, 2003.

of ca. 1.917 ± 0.003 Å and a 0.0 Å deviation of the Cu^{II} ion from the O_4 mean-plane are both consistent with pseudo-D_{2h} square-planar Cu^{II} and compare favorably with other structurally characterized examples of Cu^{II}-acac systems.[69,70,93,94] The structure of complex **3** also shows Cu---O distances of 2.702 and 2.545 Å, corresponding to axial interactions of the $CF_3SO_3^-$ counterions with the Cu^{II} core. The axial Cu---O distances are notably longer than typically observed for tetratragonally distorted CuO_6 complexes such as $[Cu(H_2O)_6]^{2+}$,[95−97] suggesting that the two Cu---O associations are at best weakly covalent metal−ligand interactions; spectroscopic evidence indicates that these interactions are not retained in solution (vida infra). As expected, significantly shorter metal−oxygen bonds (ca. 0.3 Å) are observed for the tetrahedral coordination environment of complex **6** due to the smaller ionic radius of Be^{II}.[71] The internal geometries of the Re(bpy)$(CO)_3$ and Re(tmb)$(CO)_3$ moieties in complexes **3** and **6** exhibit the pseudo-C_{3v} coordination environment common to Re^I complexes in this class;[98−101] the similarities between the two structures further indicate that the geometry within the fragment is insensitive to changes in the substituents of the polypyridyl ligand. Complex **6** exhibits a shorter $Re^I\cdots M^{II}$ distance (ca. 0.3 Å), which can be attributed to the smaller radius of the Be^{II} ion and the concomitant decrease in metal−oxygen bond lengths relative to complex **3**. Despite these differences there is considerable structural homology between the two complexes, underscoring the appropriateness of using Be^{II} as an electronically benign replacement for Cu^{II} in these systems.

Electronic Absorption Spectroscopy. The electronic absorption spectra of complexes **1**−**10** were acquired in room-temperature CH_2Cl_2 solution. Spectra for complexes **3** and **8** are shown in Figure 2; all 10 spectral profiles can be found in the Supporting Information (Figure S1). Re^I polypyridyl complexes exhibit a $^1A_1 \rightarrow {}^1$MLCT ($t_{2g} \rightarrow \pi^*$ (bpy′)) transition in the range of 330 to 430 nm depending on the substituents of the bpy′ ligand,[102,103] with electron-donating and -withdrawing groups shifting λ_{max} for this feature to the blue and red, respectively. In the present series, the absorption maximum systematically shifts from ca. 350 nm for the tmb-containing complexes (**1** and **6**) to ca. 400 nm in the Re^I-deeb analogues (**5** and **10**). The presence of charge-transfer transitions associated with the Cu^{II} core in the ultraviolet (Figure S2) gives rise to differences in this region between these adducts and their corresponding Be^{II} analogues. Nevertheless, the general similarities among these spectra, particularly with regard to the $^1A_1 \rightarrow {}^1$MLCT absorption of the Re^I-bpy′ chromophores, are suggestive

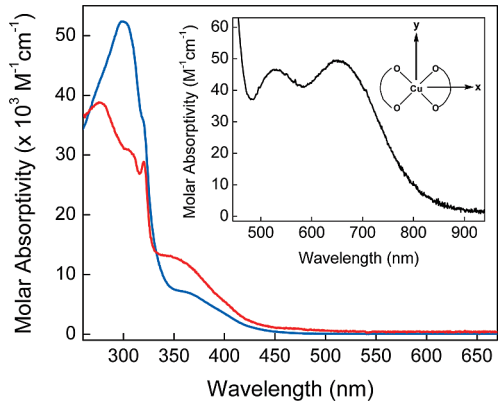

Figure 2. Electronic absorption spectra of $[Cu(pyacac)_2(Re(bpy)(CO)_3)_2](OTf)_2$ (**3**) (red trace) and $[Be(pyacac)_2(Re(bpy)(CO)_3)_2](OTf)_2$ (**8**) (blue trace) acquired in room-temperature CH_2C1_2 solution. The inset illustrates the electronic absorption spectrum of $Cu(phacac)_2$ in CH_2Cl_2 solution highlighting the ligand-field absorptions of the Cu(II) ion; the full spectrum of this compound is shown in Figure S2.

of minimal electronic coupling between these groups and the Cu^{II} center in complexes **1**−**5**.

In addition to the Re^I-based charge-transfer transitions, the $CuRe_2$ complexes also possess ligand-field transitions associated with the square-planar CuO_4 core. The low-energy tails of the charge-transfer transitions associated with the Re^I chromophores largely obscure these absorptions in compounds **1**−**10**; however, the electronic absorption spectrum of $Cu(phacac)_2$ allows for an examination of these mid-visible d−d bands (Figure 2, inset). The two peaks at 530 nm ($\varepsilon = 47\ M^{-1}\ cm^{-1}$) and 652 nm ($\varepsilon = 50\ M^{-1}\ cm^{-1}$) arise from four spin-allowed ligand-field transitions corresponding to $d_{xz} \rightarrow d_{xy}$, $d_{yz} \rightarrow d_{xy}$, $d_{z^2} \rightarrow d_{xy}$, and $d_{x^2-y^2} \rightarrow d_{xy}$ based on the polarized single-crystal absorption spectrum of $Cu(phacac)_2$[104] and the coordinate system shown in Figure 2. This spectrum, which accurately reflects the optical properties of the $Cu^{II}O_4$ core of complexes **1**−**5**, will therefore provide the basis for the spectral overlap analysis to be described later.

It should be noted that the structure of complex **3** shown in Figure 1 reveals two $CF_3SO_3^-$ counterions interacting with the Cu^{II} core. If retained in solution, these interactions would be expected to alter the absorption profile of the Cu^{II} core in complexes **1**−**5** and negate the utility of the $Cu(phacac)_2$ spectrum as a spectroscopic surrogate for the acceptor in the $CuRe_2$ series.[105] This issue was examined by titrating a CH_2Cl_2 solution of $Cu(phacac)_2$ with $(NEt_4)(CF_3SO_3)$. Addition of up to 40 equiv of triflate did not cause any discernible change in the absorption spectrum of $Cu(phacac)_2$, indicating that $CF_3SO_3^-$ is not associating with the Cu^{II} center in solution.

Steady-State and Time-Resolved Emission. Emission spectra for the $CuRe_2$ and $BeRe_2$ complexes were obtained in room-temperature deoxygenated CH_2Cl_2 solutions (Figure S3). The spectral profiles for all of the compounds correspond well to previously reported photophysical data on Re^I polypyridyl systems, with the emission originating from the ^{3}MLCT $\rightarrow {}^1A_1$ transition.[106] Emission maxima for the tmb (524 nm), dmb (550 nm), bpy (568 nm), dclb (600 nm), and deeb (620 nm) derivatives reflect the expected trend in zero-point energy of the ^{3}MLCT state based on the electron-donating and -withdrawing behavior of the substituents on the polypyridyl ligands.

(93) Maverick, A. W.; Fronczek, F. R.; Maverick, E. F.; Billodeaux, D. R.; Cygan, Z. T.; Isovitsch, R. A. *Inorg. Chem.* **2002**, *41*, 6488.
(94) Chen, B.; Fronczek, F. R.; Maverick, A. W. *Inorg. Chem.* **2004**, *43*, 8209.
(95) Gallucci, J. C.; Gerkin, R. E. *Acta Crystallogr.* **1989**, *C45*, 1279.
(96) Blackburn, A. C.; Gallucci, J. C.; Gerkin, R. E. *Acta Crystallogr.* **1991**, *C47*, 2019.
(97) Cotton, F. A.; Daniels, L. M.; Murillo, C. A.; Quesada, J. F. *Inorg. Chem.* **1993**, *32*, 4861.
(98) Lucia, L. A.; Abboud, K.; Schanze, K. S. *Inorg. Chem.* **1997**, *36*, 6224.
(99) Chen, P.; Curry, M.; Meyer, T. J. *Inorg. Chem.* **1989**, *28*, 2271.
(100) Wenger, O. S.; Henling, L. M.; Day, M. W.; Winkler, J. R.; Gray, H. B. *Inorg. Chem.* **2004**, *43*, 2043.
(101) Busby, M.; Liard, D. J.; Motevalli, M.; Toms, H.; Vlček, A. *Inorg. Chim. Acta* **2004**, *357*, 167.
(102) Sacksteder, L.; Zipp, A. P.; Brown, E. A.; Streich, J.; Demas, J. N.; DeGraff, B. A. *Inorg. Chem.* **1990**, *29*, 4335.
(103) Worl, L. A.; Duesing, R.; Chen, P.; Della Ciana, L.; Meyer, T. J. *J. Chem. Soc., Dalton Trans.* **1991**, 849.
(104) Belford, R. L.; Carmichael, J. W., Jr. *J. Chem. Phys.* **1967**, *46*, 4515.
(105) Funck, L. L.; Ortolano, T. R. *Inorg. Chem.* **1968**, *7*, 567.
(106) Striplin, D. R.; Crosby, G. A. *Chem. Phys. Lett.* **1994**, *221*, 426.

Table 3. Photophysical Data for $[M(pyacac)_2(Re(bpy')(CO)_3)_2](OTf)_2$ (complexes **1**−**10**)

compound	λ_{em} (nm)	E_{00} (cm^{-1})[a]	Φ_r	k_{obs} (s^{-1})[b]	k_r ($\times 10^5$ s^{-1})[c]	k_{nr} ($\times 10^6$ s^{-1})[d,e]
$[Cu(pyacac)_2(Re(tmb)(CO)_3)_2](OTf)_2$ (**1**)	[f]	[f]	[g]	$(6.7 \pm 0.3) \times 10^7$	[f]	67 ± 4
$[Be(pyacac)_2(Re(tmb)(CO)_3)_2](OTf)_2$ (**6**)	524	19 900	0.63	$(5.0 \pm 0.3) \times 10^5$	3.2 ± 0.2	0.19 ± 0.01
$[Cu(pyacac)_2(Re(dmb)(CO)_3)_2](OTf)_2$ (**2**)	[f]	[f]	[g]	$(1.2 \pm 0.1) \times 10^8$	[f]	120 ± 6
$[Be(pyacac)_2(Re(dmb)(CO)_3)_2](OTf)_2$ (**7**)	550	19 200	0.25	$(1.6 \pm 0.1) \times 10^6$	4.0 ± 0.2	1.2 ± 0.1
$[Cu(pyacac)_2(Re(bpy)(CO)_3)_2](OTf)_2$ (**3**)	[f]	[f]	[g]	$(1.2 \pm 0.1) \times 10^8$	[f]	120 ± 6
$[Be(pyacac)_2(Re(bpy)(CO)_3)_2](OTf)_2$ (**8**)	568	18 750	0.18	$(1.9 \pm 0.1) \times 10^6$	3.4 ± 0.2	1.6 ± 0.1
$[Cu(pyacac)_2(Re(dclb)(CO)_3)_2](OTf)_2$ (**4**)	[f]	[f]	[g]	$(1.8 \pm 0.1) \times 10^8$	[f]	180 ± 10
$[Be(pyacac)_2(Re(dclb)(CO)_3)_2](OTf)_2$ (**9**)	600	17 650	0.03	$(8.8 \pm 0.5) \times 10^6$	2.6 ± 0.1	8.5 ± 0.4
$[Cu(pyacac)_2(Re(deeb)(CO)_3)_2](OTf)_2$ (**5**)	[f]	[f]	[g]	$(2.0 \pm 0.1) \times 10^8$	[f]	200 ± 10
$[Be(pyacac)_2(Re(deeb)(CO)_3)_2](OTf)_2$ (**10**)	620	16 900	0.07	$(4.0 \pm 0.2) \times 10^6$	2.8 ± 0.2	3.7 ± 0.2

[a] Zero-point energy difference between ^{3}MLCT excited state and ground state derived from a spectral fitting analysis. [b] Error bars on k_{obs} represent the standard deviation (2σ) of five independent measurements. [c] $k_r = k_{obs} \cdot \Phi_r$. [d] $k_{nr}^{CuRe_2} = k_{obs}^{CuRe_2} - k_r^{BeRe_2}$. [e] $k_{nr}^{BeRe_2} = k_{obs}^{BeRe_2} - k_r^{BeRe_2}$. [f] This value is not quoted due to the presence of an emissive impurity, but is expected to be identical to the corresponding Be^{II} complex. [g] Radiative quantum yields for the $CuRe_2$ complexes are not reported due to the presence of an emissive impurity; however, they can be approximated by multiplying the value of Φ_r for the corresponding Be^{II} complex by the ratio of the observed decay rate constants (i.e., $k_{obs}^{BeRe_2}/k_{obs}^{CuRe_2}$).

Likewise, the radiative quantum yields (Φ_r) for complexes **6**−**10** (Table 3) are all comparable to the reported values for the corresponding mononuclear Re^I polypyridyl derivatives.[72]

The data on complexes **1**−**5** reveal that the emission intensities for the Cu^{II}-containing compounds are significantly attenuated compared to the $BeRe_2$ model complexes. Unfortunately, radiative quantum yields for complexes **1**−**5** were found to be analytically unreliable due to a small amount of an emissive impurity present in solutions of these compounds. $Cu(phacac)_2$ was determined to be nonemissive in room-temperature CH_2Cl_2 solution: the impurity is therefore likely due to the presence of *fac*-$[Re(bpy')(CO)_3(pyacac)]$ generated by displacement of the pyacac ligand by residual amounts of H_2O contained in the CH_2Cl_2. The drying and distilling procedures that were employed were exhausted until no water was detectable by ^{1}H NMR, but the low concentration of the $CuRe_2$ compound used for the emission measurements means that even trace amounts of H_2O could be sufficient to generate a small amount of dissociated species. A similar problem was encountered in our previous study of $FeRe_3$ assemblies;[41] as in that system, the presence of this emissive component proves to be inconsequential for the ensuing analysis.[107]

Quantitative information concerning emission quenching by the Cu^{II} center in complexes **1**−**5** was obtained via time-resolved emission spectroscopy. Data for the $BeRe_2$ model complexes could be fit to single-exponential decay kinetic models; emission traces and values for the observed decay rates for all five $BeRe_2$ complexes are given in Figure S4 and Table 3, respectively. As with the quantum yields, the observed excited-state lifetimes are consistent with an assignment of ^{3}MLCT → $^1A_1$ emission.[72,108] The kinetics reveal that the reduction in quantum yield across the series is due primarily to an increase in the nonradiative decay rate for ^{3}MLCT relaxation (k_{nr}) as opposed to significant variations in radiative coupling to the ground state. The only deviation from this trend is the smaller value of k_{nr} for complex **10**. This is most likely due to the additional conjugation present in the π system of the deeb ligand, which allows for increased delocalization of the π^*-based excited state relative to other members of the series. This increased delocalization is expected to give rise to a smaller net displacement of the ground- and excited-state potential energy surfaces, which in turn leads to a decrease in the rate of nonradiative decay.[73,81,82,109]

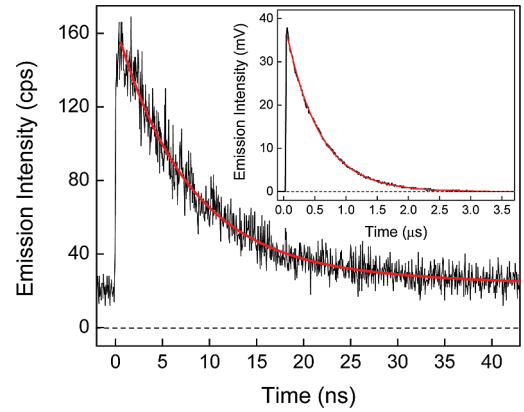

Figure 3. Time-correlated single-photon counting (TCSPC) emission data for $[Cu(pyacac)_2(Re(bpy)(CO)_3)_2](OTf)_2$ (**3**) acquired in room-temperature deoxygenated CH_2Cl_2 solution. The emission was monitored at λ_{probe} = 570 nm following excitation at λ_{pump} = 355 nm. The solid red line corresponds to a fit to a biexponential decay model with $\tau_1 = 8.2 \pm 0.4$ ns and τ_2 = 540 ns (fixed); the latter corresponds to emission from $Re(bpy)(CO)_3(pyacac)$ present in solution as a trace impurity. The inset shows nanosecond time-resolved emission data for the corresponding model complex, $[Be(pyacac)_2(Re(bpy)(CO)_3)_2](OTf)_2$ (**8**), with τ_{obs} = 540 ± 30 ns.

Analogous measurements on the nanosecond time-scale for the $CuRe_2$ complexes failed to reveal any signals beyond those of the trace impurity mentioned above. Consequently, time-correlated single-photon counting (TCSPC) was employed to measure the excited-state lifetime of the Cu^{II}-containing complexes (**1**−**5**). A plot of the TCSPC data obtained for complex **3** in deoxygenated CH_2Cl_2 solution is shown in Figure 3; data for all five $CuRe_2$ complexes (**1**−**5**) are plotted in Figure S4 and listed in Table 3. The observed time constants for excited-state decay for complexes **1**−**5** are all significantly larger than the corresponding $BeRe_2$ model complexes, ranging from a factor of ca. 20 in the case of complex **4** to more than 2 orders of magnitude for complex **1**. The signal-to-noise ratio for the

(107) It should be noted that the presence of this emissive impurity is explicitly incorporated in the kinetic models used to fit the time-resolved emission data.

(108) Kestell, J. D.; Williams, Z. L.; Stultz, L. K.; Claude, J. P. *J. Phys. Chem. A* **2002**, *106*, 5768.

(109) Barqawi, K. R.; Murtaza, Z.; Meyer, T. J. *J. Phys. Chem.* **1991**, *95*, 47.

Scheme 2

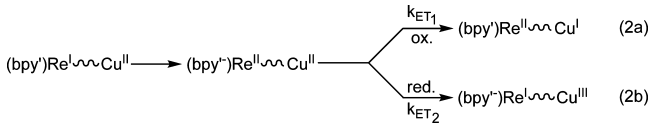

TCSPC data is relatively poor owing to a combination of significant quenching of the Re^{I}-based ^{3}MLCT states coupled with radiative rate constants for emission on the order of 10^{5} s^{-1}. Nevertheless, these observations clearly indicate the presence of a very efficient quenching process stemming from a reaction between the Re^{I}-based ^{3}MLCT excited state and the Cu^{II} core in the $CuRe_2$ assemblies.

Mechanistic Considerations. Electron- versus Energy-Transfer Quenching. Time-resolved emission data, while clearly revealing the presence of an excited-state reaction, generally do not provide definitive information as to the mechanistic origin of that reaction. Indeed, both electron- and energy-transfer processes can be envisioned for the Re^{I}-based ^{3}MLCT excited state. Electron transfer (k_{ET}) could in principle proceed by either oxidative (eq 2a) or reductive (eq 2b) quenching to produce Cu^{I} or Cu^{III} as photoproducts (Scheme 2). In order to determine if electron transfer is thermodynamically viable, the electrochemical properties for the $CuRe_2$ as well as the $BeRe_2$ analogues were measured. Cyclic and differential pulse voltammograms for complexes **1**−**10** were recorded in CH_3CN solution; the data are listed in Table 4.[110] The availability of the Be^{II} model complexes considerably simplifies the process of assigning many of the electrochemical properties of all 10 complexes due to the redox-inert nature of this ion. Accordingly, the single reduction waves can be immediately ascribed to the bipyridyl ligand of the Re moiety in each case. The positive shift in potential across the series is consistent with the more electron-withdrawing nature of the substituents as one progresses from the methyls of tmb (**6**) to the diethyl ester groups in complex **10**. Similarly, the oxidation waves are easily assigned to the Re^{I}/Re^{II} couple. The influence of the bipyridyl substitutents are apparent in these data as well, with the more electron-deficient ligand giving rise to the most positive oxidation potential for the Re center. The results are all consistent with what has been observed for complexes of the general form *fac*-[Re(4,4′-X_2-bpy)$(CO)_3$(4-Etpy)](PF_6) previously reported in the literature.[72]

In addition to the Re^{I}-based features, complexes **1**−**5** should also exhibit redox chemistry associated with the central Cu^{II} ion, which prompted the investigation of the electrochemical properties of $Cu(phacac)_2$. The electrochemical properties of $Cu(acac)_2$ and related complexes in CH_3CN solution have been previously reported,[111,112] with the Cu^{II} metal center observed to undergo highly irreversible reductive ($Cu^{II} \rightarrow Cu^{I}$) and oxidative ($Cu^{II} \rightarrow Cu^{III}$) processes. $Cu(phacac)_2$ exhibits a wave at −1.48 V in CH_3CN solution, which can be assigned to the $Cu^{II} \rightarrow Cu^{I}$ reduction; this potential shifts to −1.73 V in CH_2Cl_2. The $Cu^{II} \rightarrow Cu^{III}$ oxidation occurs at +1.31 V in CH_3CN and lies outside the solvent window of CH_2Cl_2 (i.e. >1.5 V). Although the Cu^{II} potentials are masked in certain cases by the Re^{I}- and polypyridyl-based processes, the assignments reported in Table 4 for the $CuRe_2$ series are validated by their close correspondence to the data acquired on the $BeRe_2$ systems.

The electrochemical data described above were used in conjunction with the zero-point energy gaps of the ^{3}MLCT states (E_{00}, Table 3) to determine thermodynamic driving forces for photoinduced electron transfer.[113,114] The values of ΔG^{ET} listed in Table 4 reveal that electron transfer is significantly uphill for both oxidative and reductive quenching processes in all five $CuRe_2$ complexes. Significantly, these reactions become more endothermic in CH_2Cl_2 (the solvent used for the photophysical measurements) due to the shifts in the Cu^{II}-based redox processes indicated above. These electrochemical data therefore effectively rule out electron transfer as a viable quenching mechanism for the $CuRe_2$ series.

On the basis of the analysis presented above, the most likely explanation for ^{3}MLCT quenching in all five of the $CuRe_2$ assemblies is excited-state energy transfer. Regardless of the specific mechanism (vide infra), energy transfer from the ^{3}MLCT state of the Re^{I}-bpy′ moiety to the Cu^{II} core should result in the formation of ligand-field excited state(s) of the latter; direct observation of these excited state(s) is far and away the best means of definitively establishing this energy-transfer process. Irradiation into the ligand-field states of $Cu(phacac)_2$ in degassed CH_2Cl_2 solution did not give rise to any detectable emission, leaving transient absorption spectroscopy as the only viable probe available for monitoring formation of the Cu^{II}-based excited state(s). Femtosecond time-resolved absorption measurements were therefore carried out on $Cu(phacac)_2$ in CH_2Cl_2 solution in order to determine the spectral region where these excited states would absorb in the $CuRe_2$ assemblies. A broad, extremely weak transient ($\Delta A < 10^{-3}$) having a lifetime on the order of several picoseconds was observed in the visible following excitation at both 450 and 650 nm. The feature was too weak to allow for a detailed analysis, but the intensity and lifetime were qualitatively consistent with our expectations for a ligand-field excited state. Analogous measurements were then carried out on complex **3**. Strong signals associated with the ^{3}MLCT excited state of the Re^{I}-bpy chromophore[41] were observed to undergo simultaneous decay consistent with the ca. 8 ns lifetime determined via TCSPC. No signal corresponding to a Cu^{II} excited-state species was detected.

To understand what, if anything, this observation implies, it is important to consider the relative magnitudes of the rate constants for energy transfer and the excited-state lifetime of the Cu^{II} acceptor. In transient absorption spectroscopy, there must be a sufficient concentration of excited-state species present in order for it to be detected. How much is needed is obviously dependent upon a number of factors (the sensitivity of the instrument, relative molar absorptivities of the ground and

(110) The cyclic voltammetry measurements were performed in CH_3CN due to insufficient solubility of the $CuRe_2$ complexes in CH_2Cl_2 solution. The validity of using redox potentials measured in CH_3CN to evaluate driving forces for electron transfer in CH_2Cl_2 solutions is based in part on our previously reported data on analogous $FeRe_3$/$AlRe_3$ complexes (cf. 41), which reveal that the redox properties of the Re^{I}-bpy′ fragment differ by less than 10 mV between these two solvents. The impact of the change in solvent on the redox properties of the Cu^{II} center is addressed in the text.

(111) Gritzner, G.; Murauer, H.; Gutmann, V. *J. Electroanal. Chem. Interfacial Electrochem.* **1979**, *101*, 177.

(112) Bradbury, J. R.; Hampton, J. L.; Martone, D. P.; Maverick, A. W. *Inorg. Chem.* **1989**, *28*, 2392.

(113) Rehm, D.; Weller, A. *Isr. J. Chem.* **1970**, *8*, 259.

(114) Forms of the Rehm−Weller equation employed to characterize the oxidative and reductive quenching processes were $\Delta G_{ET}^{ox} = E_{ox}(Re^{I/II}) - E_{red}(Cu^{II/I}) - E_{00}$ and $\Delta G_{ET}^{red} = E_{ox}(Cu^{II/III}) - E_{red}(bpy'^{0/-}) - E_{00}$, respectively, where E_{00} is the energy gap between the ground and lowest-energy ^{3}MLCT excited state of the donor. In both cases, the small work term typically employed for bimolecular systems was not included in the analysis.

Table 4. Electrochemical Data and Calculated Electron Transfer Driving Forces (ΔG^{ET}) for Complexes **1**−**10**

	electrochemical potential (V)			
compound	E_{ox} ($Re^{I/II}$)[c]	E_{red} ($bpy'^{0/-}$)[c]	ΔG^{ET}_{ox} (eV)[a]	ΔG^{ET}_{red} (eV)[b]
$[Cu(pyacac)_2(Re(tmb)(CO)_3)_2](OTf)_2$ (**1**)	+1.30	−1.83	+0.31	+0.67
$[Be(pyacac)_2(Re(tmb)(CO)_3)_2](OTf)_2$ (**6**)	+1.28	−1.81		
$[Cu(pyacac)_2(Re(dmb)(CO)_3)_2](OTf)_2$ (**2**)	+1.31	−1.71	+0.41	+0.64
$[Be(pyacac)_2(Re(dmb)(CO)_3)_2](OTf)_2$ (**7**)	+1.31	−1.68		
$[Cu(pyacac)_2(Re(bpy)(CO)_3)_2](OTf)_2$ (**3**)	+1.36	−1.61	+0.52	+0.60
$[Be(pyacac)_2(Re(bpy)(CO)_3)_2](OTf)_2$ (**8**)	+1.34	−1.57		
$[Cu(pyacac)_2(Re(dclb)(CO)_3)_2](OTf)_2$ (**4**)	+1.41	−1.38	+0.70	+0.50
$[Be(pyacac)_2(Re(dclb)(CO)_3)_2](OTf)_2$ (**9**)	+1.44	−1.34		
$[Cu(pyacac)_2(Re(deeb)(CO)_3)_2](OTf)_2$ (**5**)	+1.51	−1.23	+0.89	+0.44
$[Be(pyacac)_2(Re(deeb)(CO)_3)_2](OTf)_2$ (**10**)	+1.50	−1.19		
	E_{ox} ($Cu^{II/III}$)[c]	E_{red} ($Cu^{II/I}$)		
$Cu(phacac)_2$	+1.31	−1.48[c] (−1.73[d])		

[a] Calculated using the electrochemical data for $Cu^{II} \rightarrow Cu^{I}$ in $Cu(phacac)_2$ in CH_3CN as the reduction potential of the acceptor. The driving force in CH_2Cl_2 solution will be more endothermic by ca. 0.2 eV due to the positive shift in the $Cu^{II/I}$ potential in CH_2Cl_2 relative to CH_3CN. [b] Calculated using the electrochemical data for $Cu^{II} \rightarrow Cu^{III}$ in $Cu(phacac)_2$ in CH_3CN as the oxidation potential of the acceptor. [c] Measured in CH_3CN solution. [d] Measured in CH_2Cl_2 solution.

excited state(s) involved, etc.), but concentrations on the order of 1−10% relative to the ground state are typical. In the case of the $CuRe_2$ assemblies, the rate of energy transfer (as inferred by the quenching of the ^{3}MLCT excited state of the Re^I chromophore) is several orders of magnitude slower than the rate of decay expected for the Cu^{II}-based excited state. This disposition of relative rates will result in disappearance of the excited ligand-field state(s) of the Cu^{II} acceptor immediately upon its formation. This fact coupled with the anticipated weakness of the signal and the strength of the features associated with the Re^I chromophore will conspire to make it extremely difficult if not impossible to directly observe the excited state(s) of the Cu^{II} acceptor subsequent to energy transfer. Despite the inability to directly detect the Cu^{II}-based excited state, we are nevertheless confident in our assignment of quenching of the Re^I-based ^{3}MLCT excited state to an energy-transfer process based on the endothermicity of the two possible electron-transfer pathways as well as our previous study of analogous $FeRe_3$ assemblies.[41]

The two most important mechanisms for energy transfer are electron superexchange (Dexter)[115] and dipole−dipole coupling (Förster).[116] Dexter energy transfer is subject to a distance dependence that falls off as e^{-2r} due to its reliance on orbital overlap. As such, it is usually relegated to covalently linked systems in which the donor and acceptor lie in close proximity and are electronically coupled. Förster transfer is a through-space mechanism that occurs when the donor emission nonradiatively couples to an absorptive feature of the acceptor. The dipolar nature of this interaction gives rise to a shallower r^{-6} distance dependence, allowing this mechanism to be operative over much longer distances.[117] The X-ray structure data for complex **3** shows a $Re^I \cdots Cu^{II}$ separation of nearly 10 Å, a value that lies at the limit of what is typically considered for an exchange-based process.[46,118−120] The similarity in the charge-transfer region between the absorption spectra of complexes **1**−**5** and their respective $BeRe_2$ analogues, as well as their electrochemical properties, suggests minimal electronic coupling exists between the Re^I and Cu^{II} subunits. This point is amplified by the computational results of Meyer and co-workers, which reveal that the majority of the amplitude associated with the thermalized ^{3}MLCT wave function for complexes of the form *fac*-[Re(4,4′-X_2bpy)$(CO)_3$(4-Etpy)](PF_6) (X = CH_3, H, and CO_2Et) is concentrated within the π^* levels of the 4,4′-X_2bpy derivatives and less so on the 4-Etpy ligand.[121] This situation limits the possibility of significant through-bond electronic coupling between the Re^I charge-transfer excited states and the Cu^{II} metal centers. This combination of structural and electronic characteristics of the $CuRe_2$ series therefore makes it unlikely that Dexter-type exchange is playing a dominant role in the energy-transfer dynamics of these systems. Consequently, we assign the energy-transfer process in these $CuRe_2$ assemblies as arising from a Förster-type dipole−dipole coupling mechanism.[122]

Spectral Overlap Analysis: State-Selective Energy Transfer. The classic equation describing the Förster energy-transfer rate constant (k_{EnTr}) is given in eq 3,[123]

(115) Dexter, D. L. *J. Chem. Phys.* **1953**, *21*, 836.
(116) Förster, T. *Discuss. Faraday Soc.* **1959**, *27*, 7.
(117) Yardley, J. T. *Introduction to Molecular Energy Transfer*; Academic Press: New York, 1980.
(118) Wang, Y.; Schanze, K. S. *Inorg. Chem.* **1994**, *33*, 1354.
(119) Berg, K. E.; Tran, A.; Raymond, M. K.; Abrahamsson, M.; Wolny, J.; Redon, S.; Andersson, M.; Sun, L.; Styring, S.; Hammarström, L.; Toftlund, H.; Åkermark, B. *Eur. J. Inorg. Chem.* **2001**, 1019.
(120) Soler, M.; McCusker, J. K. *J. Am. Chem. Soc.* **2008**, *130*, 4708.
(121) Dattelbaum, D. M.; Martin, R. L.; Schoonover, J. R.; Meyer, T. J. *J. Phys. Chem. A* **2004**, *108*, 3518.
(122) A question was raised by one reviewer concerning the validity of using a dipolar model to describe the energy-transfer dynamics in this class of compounds. For intramolecular systems it is certainly the case that one needs to question whether a point-dipole approximation is appropriate (for example, see: Wong, K. F.; Bagchi, B.; Rossky, P. J. *J. Phys. Chem. A* **2004**, *108*, 5752). In the present system, however, the successful quantitative application of Förster theory for the $FeRe_3$ analogues described in ref 41 coupled with the smaller transition dipoles associated with the ligand-field acceptor states of the Cu^{II} core significantly mitigates these concerns.
(123) Van Der Meer, B. W.; Coker, G. I.; Chen, S.-Y. *Resonance Energy Transfer, Theory and Data*; VCH Publishers: New York, 1994.

$$k_{EnTr} = \frac{9000 \ln(10)\kappa^2 k_r J}{128\pi^5 \eta^4 N_A R^6} \quad (3)$$

where κ^2 is the dipole orientation factor, k_r is the radiative rate constant of the donor, J is the spectral overlap integral, η is the refractive index of the solvent, N_A is Avogadro's number, and R is the donor−acceptor separation. The spectral overlap integral essentially quantifies the resonance condition for energy transfer and can be evaluated from the spectroscopic properties of the system using eq 4,

$$J = \int_0^\infty \frac{\bar{F}_D(\bar{\nu})\, \bar{\varepsilon}_A(\bar{\nu})}{\bar{\nu}^4} d(\bar{\nu}) \quad (4)$$

where $\bar{F}_D$ is the normalized emission spectrum of the donor and $\bar{\varepsilon}_A$ is the absorption profile of the acceptor in units of molar absorptivity. A plot of the emission spectra of complexes **6** through **10** superimposed on the visible absorption spectrum of Cu(phacac)$_2$ is shown in Figure 4. It can be seen that the systematic shift in the emission maximum across the series results in a modulation of the overlap between the donor and the acceptor. As mentioned previously, the absorption spectrum of the Cu^{II} acceptor consists of a ligand-to-metal charge-transfer feature in the blue/near-ultraviolet region, as well as ligand-field transitions in the mid-visible; substituent changes on the bpy′ ligands serve to tune the resonance between the ^{3}MLCT emission of the Re^I-bpy′ fluorophore and these various acceptor state(s).

The Förster model defines a proportionality between the spectral overlap integral and the rate of energy transfer subject to variations in the donor−acceptor distance, the intrinsic radiative lifetime of the donor, and the relative orientation of the coupled transition dipoles (κ^2). In viewing the series of complexes **1** through **5** as a whole, several of these variables can be accounted for explicitly as a means of examining trends in the rate of energy transfer. The availability of the BeRe$_2$ model complexes affords values of k_r for each compound in the series. We can therefore write an expression for the rate of energy transfer normalized for the rate of radiative decay as

$$\frac{k_{EnTr}}{k_r} = C\kappa^2 J \quad (5a)$$

where C represents the collection of constants from the Förster equation (including the r^{-6} donor−acceptor distance term). Our previous study on Fe^{III}-containing assemblies[41] demonstrated that one could use information from single-crystal X-ray structures in conjunction with reasonable estimates for the positions of the relevant transition dipole vectors to calculate κ^2 explicitly. In the present case, the metal-localized nature of the d−d states on the Cu^{II} center makes this approach more difficult (vide infra); however, we can invert this process and calculate values for κ^2 based on our experimental data. Values for k_{EnTr}/k_r, the overlap integral (J_{total}), and κ^2 for compounds **1**−**5** are listed in Table 5. These numbers reveal the surprising result that the value of κ^2 is not constant across the series. Using a donor−acceptor distance of 10.37 Å (a value corresponding to the distance between the Cu^{II} center and the midpoint of a vector that bisects the N−Re−N bond angle[41]), κ^2 for compound **1** is found to be 2.8, whereas for compound **5** the corresponding value is 5.7; this latter result exceeds the maximum value of $\kappa^2 = 4$ calculated for head-to-tail parallel transition dipoles.[116]

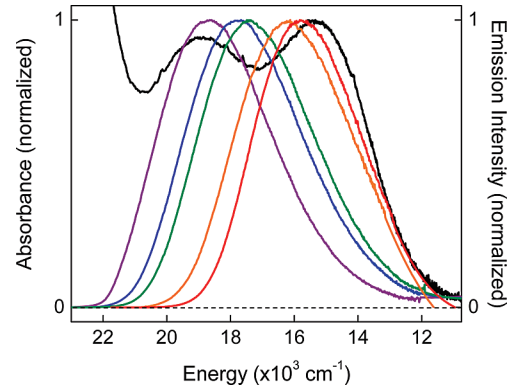

Figure 4. Overlay of the emission spectra of [Be(pyacac)$_2$(Re(tmb)-(CO)$_3$)$_2$](OTf)$_2$ (**6**, purple), [Be(pyacac)$_2$(Re(dmb)(CO)$_3$)$_2$](OTf)$_2$ (**7**, blue), [Be(pyacac)$_2$(Re(bpy)(CO)$_3$)$_2$](OTf)$_2$ (**8**, green), [Be(pyacac)$_2$(Re(dclb)-(CO)$_3$)$_2$](OTf)$_2$ (**9**, orange), and [Be(pyacac)$_2$(Re(deeb)(CO)$_3$)$_2$](OTf)$_2$ (**10**, red) with the electronic absorption spectrum of Cu(phacac)$_2$. All of the spectra were acquired in CH_2Cl_2 solutions.

The underlying reason for the apparent disconnect between the predictions of eq 5a and the results obtained for compounds **1** through **5** can be understood by examining the normalized rates of energy transfer across the series in a slightly different manner. For any two members of the series i and j, we can write the following expression for the relative change in the rate of energy transfer as a function of spectral overlap:

$$\frac{[k_{EnTr}/k_r]_j}{[k_{EnTr}/k_r]_i} = \frac{C_j\kappa_j^2 J_j}{C_i\kappa_i^2 J_i} \quad (5b)$$

The isostructural nature of compounds **1** through **5** implies that, to a reasonable degree of precision, the donor−acceptor distance is essentially constant across the series.[124] Cancellation of these terms affords eq 5c:

$$\frac{[k_{EnTr}/k_r]_j}{[k_{EnTr}/k_r]_i} = \frac{\kappa_j^2 J_j}{\kappa_i^2 J_i} \quad (5c)$$

This expression indicates that the relative rates of (k_r-normalized) energy transfer should correlate with the ratio of their spectral overlap integrals weighted by a proportionality constant equal to the relative magnitudes of their orientation factors: dipolar coupling involving the same two states (i.e., the ^{3}MLCT state of the Re-bpy′ moieties and the Cu^{II} acceptor) should therefore yield a slope of 1 since their orientation factors will cancel. Using the data for compound **1** as our ith reference state we find that κ^2_j/κ^2_1 increases from 1.18 for compound **2** to 2.03 for compound **5**. These data confirm the trend suggested by the individual κ^2 values listed in Table 5, namely, that the orientation factor associated with energy transfer in this system is different in one region of the spectrum versus another. Specifically, our analysis reveals a net increase in the rate of energy transfer as the donor emission comes into resonance with the low-energy portion of the Cu^{II} absorption profile.

(124) The degree to which a given substituent is electron donating or electron withdrawing is expected to subtly modulate the spatial characteristics of the ^{3}MLCT excited state of the Re-bpy′ group. However, our previous study of FeRe$_3$ assemblies (cf. 41) demonstrated that these variations are minor given the scale of the distances involved in energy transfer in these types of systems.

Table 5. Calculated Spectral Overlap Integrals and Energy Transfer Rate Constants for Complexes **1**−**5**

compound	J_{total}[a]	J_{G1}[a]	J_{G2}[a]	J_{G3}[a]	k_{EnTr} ($\times 10^8$ s^{-1})[b]	k_{EnTr}/k_r[c]	κ^{2}[d]
$[Cu(pyacac)_2(Re(tmb)(CO)_3)_2](OTf)_2$ (**1**)	4.29	0.127	2.26	1.90	0.67	208	2.8
$[Cu(pyacac)_2(Re(dmb)(CO)_3)_2](OTf)_2$ (**2**)	5.14	0.046	2.07	3.03	1.18	295	3.3
$[Cu(pyacac)_2(Re(bpy)(CO)_3)_2](OTf)_2$ (**3**)	5.52	0.027	1.92	3.57	1.18	347	3.7
$[Cu(pyacac)_2(Re(dclb)(CO)_3)_2](OTf)_2$ (**4**)	6.68	0.0045	1.29	5.39	1.71	658	5.7
$[Cu(pyacac)_2(Re(deeb)(CO)_3)_2](OTf)_2$ (**5**)	7.09	0.0014	0.97	6.12	1.96	700	5.7

[a] Reported in units of 10^{-16} M^{-1} cm^3. [b] $k_{EnTr} = k_{obs}^{CuRe_2} - k_{obs}^{BeRe_2}$ (Table 3). [c] Values for k_r were taken from the corresponding $BeRe_2$ complex (Table 3). [d] Calculated using eq 5a with $R = 10.37$ Å.

In order to determine whether there are, in fact, differential contributions from the excited-state manifold of Cu^{II} to the energy-transfer dynamics of this system, we deconvolved the absorption profile of $Cu(phacac)_2$ into a sum of Gaussians as a means of examining each portion of the compound's excited-state structure individually (Figure 5A). As expected, the spectrum is well-described by three bands corresponding to the high-energy charge-transfer feature (G1) and two, lower-intensity bands assigned to ligand-field transitions (G2 and G3).[104] Using this fitted spectrum, the total spectral overlap integral (J_{total}) can be apportioned according to its various components (where $J_{total} = J_{G1} + J_{G2} + J_{G3}$). The data in Table 5 reveal that the charge-transfer state contributes minimally to the overall spectral overlap, with contributions ranging from a high of ca. 3% in the case of compound **1** to less than 0.02% in compound **5**. This is a clear, quantitative indication that the ligand-field terms are the dominant acceptor states in this system. As the emission spectrum is tuned toward the red, the total spectral overlap increases; however, the contribution from the higher energy ligand-field transition(s) decreases from 53% in compound **1** to 14% in compound **5**. At the same time, fractional overlap with the G3 component increases from 44% to 86% of the total. Since the value of κ^2_j/κ^2_1 from eq 5c is observed to increase across the series, we can infer from this analysis that the rate of energy transfer from the ^{3}MLCT state of the Re-bpy′ moiety is intrinsically faster when coupling to the G3 component of the Cu^{II} absorption profile as compared to G2. This conclusion is further supported by noting that the ratio of orientation factors as defined by eq 5c yields the same value of 2.03 for compounds **4** and **5**, implying that $\kappa^2_5/\kappa^2_4 = 1$. Inspection of the data in Table 5 reveals an increase in J_{total} for compound **5** versus compound **4** but comparatively little change in the relative contributions of G2 and G3. In this context, the variation in κ^2 across the entire series can be interpreted in terms of differences in the orientation of the transition dipoles associated with G2 and G3: once changes in spectral overlap are isolated to G3 (i.e., compounds **4** and **5**), the proportionality factor in eq 5c collapses to unity.

The analysis presented above clearly points to a substantive difference in the nature of the excited states associated with the two observed absorption features of the Cu^{II} core in terms of their ability to engage in energy transfer from the Re-bpy′ fluorophore. We therefore carried out a time-dependent DFT calculation on $Cu(phacac)_2$ in CH_2Cl_2 solution in order to obtain a more detailed theoretical description of these states. The transition energies, oscillator strengths, and orbital compositions of the four lowest-energy excited states that are predicted from this calculation are listed in Table 6. The oscillator strengths calculated for all four transitions are consistent with the Laporte-forbidden nature of d−d absorptions. The calculated transition energies along with the absorption spectrum of $Cu(phacac)_2$ acquired in CH_2Cl_2 solution are plotted in Figure 6. The results

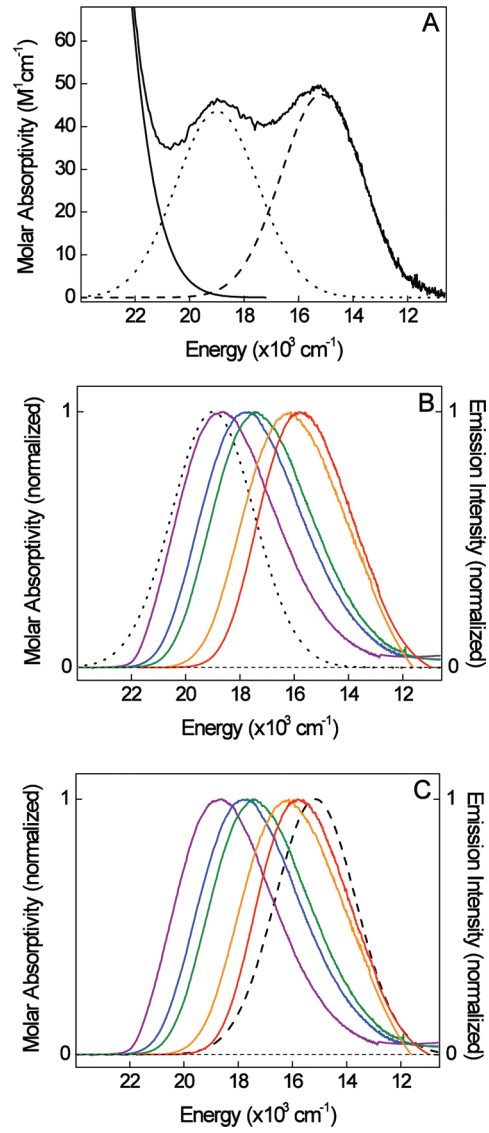

Figure 5. (A) Ground-state absorption spectrum of $Cu(phacac)_2$ in CH_2Cl_2 (black) fit with a series of three Gaussians (G1 (solid trace), G2 (dotted trace), and G3 (dashed trace)). (B and C) Overlay of the emission spectra of $[Be(pyacac)_2(Re(tmb)(CO)_3)_2](OTf)_2$ (**6**, purple), $[Be(pyacac)_2(Re(dmb)(CO)_3)_2](OTf)_2$ (**7**, blue), $[Be(pyacac)_2(Re(bpy)(CO)_3)_2](OTf)_2$ (**8**, green), $[Be(pyacac)_2(Re(dclb)(CO)_3)_2](OTf)_2$ (**9**, orange), and $[Be(pyacac)_2(Re(deeb)(CO)_3)_2](OTf)_2$ (**10**, red) with G2 and G3, respectively.

of the calculation are in reasonably good agreement with experiment, which we take as an indication of the general validity of the wave functions associated with these four absorptive features.

GaussView renderings of the orbitals involved in the four calculated excited states are shown in Figure 7. Excited States 1 (18 831 cm^{-1}), 2 (18 703 cm^{-1}), and 4 (14 778 cm^{-1}) are

Table 6. Calculated Orbital Composition of the Lowest-Energy Spin-Allowed Absorptions of $Cu(phacac)_2$ in CH_2Cl_2 solution

	E (cm^{-1})	f_{calc}[a]	orbital transitions (c_i)[b]
Excited State 1[c]	18 831	0.0000	$86\beta \rightarrow 108\beta$ (0.17) $87\beta \rightarrow 108\beta$ (0.12) $90\beta \rightarrow 108\beta$ (0.23) $96\beta \rightarrow 108\beta$ (0.94) $100\beta \rightarrow 108\beta$ (0.11)
Excited State 2[c]	18 703	0.0000	$86\beta \rightarrow 108\beta$ (0.23) $87\beta \rightarrow 108\beta$ (0.31) $97\beta \rightarrow 108\beta$ (0.92)
Excited State 3[d]	16 280	0.0000	$86\beta \rightarrow 108\beta$ (0.42) $87\beta \rightarrow 108\beta$ (0.33) $90\beta \rightarrow 108\beta$ (0.23) $100\beta \rightarrow 108\beta$ (0.85)
Excited State 4[d]	14 778	0.0000	$84\beta \rightarrow 108\beta$ (0.17) $95\beta \rightarrow 108\beta$ (0.62) $107\beta \rightarrow 108\beta$ (0.75)

[a] Calculated oscillator strength. [b] c_i corresponds to the coefficient for the specific orbital transition in the calculated absorption feature. The contribution of each component to the total wavefunction is given by c_i^2. [c] Excited States 1 and 2 comprise the G2 transition of the deconvolved spectrum in Figure 5A. [d] Excited States 3 and 4 comprise the G3 transition of the deconvolved spectrum in Figure 5A.

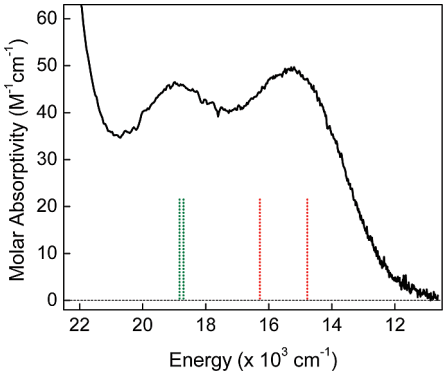

Figure 6. Four lowest-energy transitions of $Cu(phacac)_2$ determined from a TD-DFT calculation plotted against the ground-state absorption spectrum of $Cu(phacac)_2$ in CH_2Cl_2 (black). The green- and red-dotted lines represent the G2- and G3-based transitions, respectively. The calculated oscillator strengths for all four transitions are zero (Table 6); the intensities of the calculated absorptions have therefore been arbitrarily scaled to facilitate comparison with the experimental spectrum.

principally $d_{z^2} \rightarrow d_{xy}$ ($96\beta \rightarrow 108\beta$), $d_{yz} \rightarrow d_{xy}$ ($97\beta \rightarrow 108\beta$), and $d_{xz} \rightarrow d_{xy}$ ($107\beta \rightarrow 108\beta$) in origin, respectively. Excited State 3 (16 280 cm^{-1}) has a small contribution from the $90\beta \rightarrow 108\beta$ ($d_{x^2-y^2} \rightarrow d_{xy}$) transition, but is dominated by the $100\beta \rightarrow 108\beta$ (73%) component, which contains contributions from both charge-transfer and metal-centered excited states. A closer look at 100β reveals a large metal−ligand bonding component to the wave function, along with density located solely on the Cu^{II} metal center buried within this bonding contribution. The metal-centered density suggests a significant fraction of d−d character exists in the $100\beta \rightarrow 108\beta$ transition, which would explain the lack of oscillator strength associated with Excited State 3. TD-DFT calculations were also performed on $Cu(phacac)_2$ in frozen D_{2h} symmetry in a CH_2Cl_2 environment in order to compare with the results from the minimized solution-phase geometry. Results of the two TD-DFT analyses exhibited close correspondence in both energy ordering and orbital compositions for the four low-energy transitions, suggesting that the structure of $Cu(phacac)_2$ does not vary significantly between the solution-phase and idealized geometries.

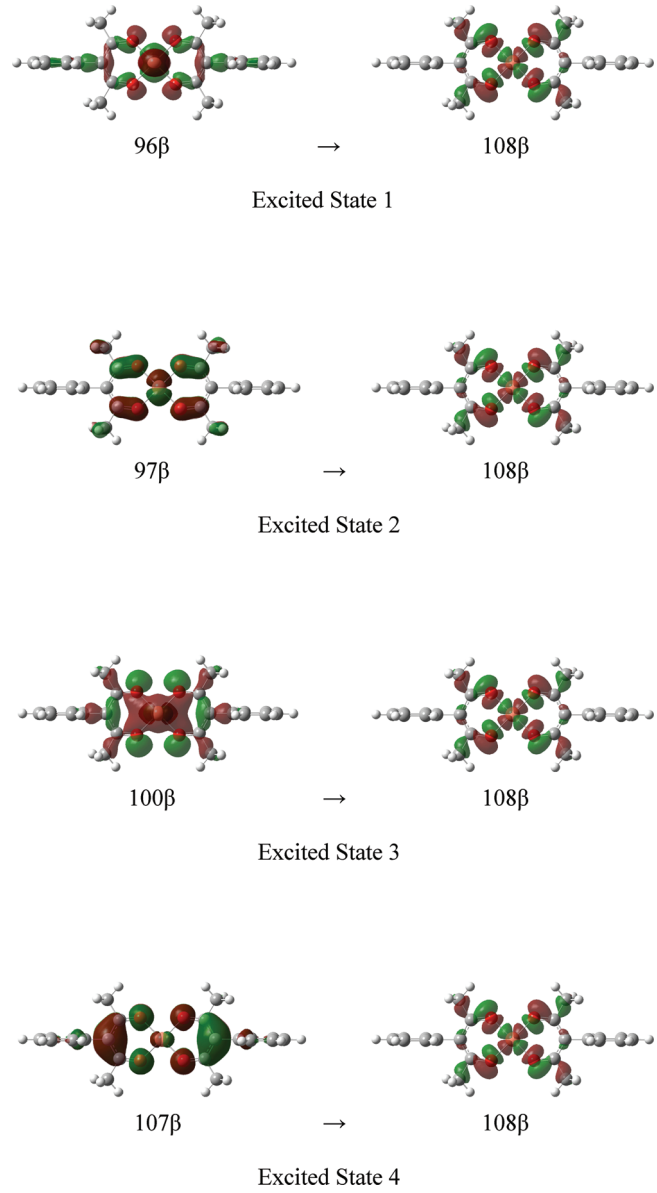

Figure 7. Drawings of the orbitals involved in the lowest-energy spin-allowed transitions of $Cu(phacac)_2$ based on a TD-DFT calculation. The coordinate system used is that shown in Figure 2 with the CuO_4 coordination environment drawn in the xy plane. See Table 6 for further details.

The analysis of the energy transfer dynamics of compounds **1** through **5** indicated a significant difference in the rate of energy transfer for coupling to the two absorption bands of the Cu^{II} absorption profile, a difference that appears to be linked to the dipole orientation factor κ^2. At first glance this would seem to be an unlikely scenario given the metal-centered nature of ligand-field absorptions; as mentioned in the Introduction, d−d acceptor states represent a nearly ideal manifestation of the point-dipole approximation inherent to Förster theory. Fleming and co-workers have demonstrated how one can use density matrix formulations to obtain detailed representations of transition dipoles for energy-transfer processes involving carotenoids.[125] The transition metal-based nature of the excited states involved in the present study makes an analogous approach difficult; however, visual inspection of the ground- and excited-

(125) Vaswani, H. M.; Hsu, C.-P.; Head-Gordon, M.; Fleming, G. R. *J. Phys. Chem. B* **2003**, *107*, 7940.

state orbital configurations reveals two interesting features. A comparison of the calculated transition energies from TD-DFT with the $Cu(phacac)_2$ ground-state absorption spectrum shows the higher-energy G2 band is dominated by the $96\beta \rightarrow 108\beta$ ($d_{z^2} \rightarrow d_{xy}$) and $97\beta \rightarrow 108\beta$ ($d_{yz} \rightarrow d_{xy}$) transitions, whereas the lower-energy G3 band is comprised mainly of the $100\beta \rightarrow 108\beta$ and the $107\beta \rightarrow 108\beta$ ($d_{xz} \rightarrow d_{xy}$) transitions. One striking difference between these transitions is the lack of an *x*-axis component in the wave functions corresponding to the occupied orbitals of the two highest-energy excited states. Ligand-field transitions—at least those arising from either d^1 or d^9 configurations where a one-electron orbital picture can be invoked—can be thought of in terms of a transfer of charge between the different planes defined by the orbital's azithumal quantum number (m_l). In this regard, the transitions contributing to the G2 feature ($d_{z^2} \rightarrow d_{xy}$ and $d_{yz} \rightarrow d_{xy}$) will be distinct in a geometric sense from the $d_{xz} \rightarrow d_{xy}$ transition that characterizes the lowest-energy feature in G3. Absent more detailed information, it is difficult to quantify whether this should give rise to an increase or decrease in dipolar coupling to the Re^I-based excited state, but it seems reasonable to expect a difference.

A second distinction between the G2 and G3 bands that could be playing a role in the observed dynamics is the nature of Excited State 3. Despite its low oscillator strength and all indications from experimental data of its ligand-field nature,[104] Figure 7 illustrates that the $100\beta \rightarrow 108\beta$ transition is qualitatively different from the other three excited states comprising the visible absorption spectrum of $Cu(phacac)_2$. On the basis of the spatial distribution of orbital 100β there appears to be some charge-transfer character to this transition, although clearly not sufficient to impact the oscillator strength for the absorption. Nevertheless, the larger change in charge distribution associated with Excited State 3 could be having a subtle influence on the magnitude of the transition dipole, which in turn would enhance the rate of energy transfer when coupling to this state. It is interesting to note the fact that the G3 feature, being composed of distinct excited states, explains at least qualitatively why the value of κ^2 calculated from eq 5a for compounds **4** and **5** was found to exceed the theoretical maximum of 4 (Table 5). Given the above analysis, each of these excited states should be viewed as an independent acceptor: coupling to both of these states as part of the overlap factor for G3 would therefore lead to an "effective" value of κ^2 (e.g., a sum of contributions) as opposed to the value one would calculate assuming a single donor−acceptor interaction. A more detailed theoretical treatment of this system would clearly be required in order to explore these ideas further.

Concluding Comments. The synthesis, structures, and photophysical properties of a series of covalently linked assemblies containing Re^I-bipyridyl donors and a Cu^{II}-acac acceptor have been described. Steady-state and time-resolved emission spectroscopies indicate that the strongly emissive Re^I-based ^{3}MLCT excited state is significantly quenched in the presence of the Cu^{II} center relative to electronically benign Be^{II} analogues. Favorable overlap between the donor emission and the visible absorption spectrum of the acceptor, coupled with a ca. 10 Å donor−acceptor separation and unfavorable driving forces for electron transfer, allowed for an assignment of Förster energy transfer as the dominant mechanism for excited-state reactivity in this system. A detailed examination of the rates of energy transfer across the series revealed that the degree of dipolar coupling between the donor and acceptor was not constant across the absorption envelope of the Cu^{II} acceptor, but instead exhibited preferential coupling to the lower-energy portion of the ligand-field manifold. Fitting the absorption spectrum of the Cu^{II} chromophore with a series of Gaussians allowed for a differential analysis of the spectral overlap that quantified differences in the dipole orientation factor κ^2 as the emission profile was tuned across the absorption spectrum of the acceptor. A TD-DFT analysis of the central Cu^{II} species revealed the composition of the Cu^{II}-based ligand-field acceptor states and permitted the identification of the specific orbitals involved in dipolar energy transfer. This study, in addition to providing a unique example of orbitally specific excited-state reactivity, also illustrates the importance of considering the substructure of absorption bands in terms of its potential impact on dipolar energy-transfer processes.

Acknowledgment. The authors wish to thank Professor Gary Blanchard for use of the time-correlated single-photon counting spectrometer and for insightful discussions, Dr. Dong Guo for acquisition and refinement of the single-crystal X-ray data for complexes **3** and **6**, Richard Fehir for assistance with the TD-DFT calculations, and Allison Brown for assistance with the ultrafast time-resolved absorption measurements. This work was supported with funds from the National Science Foundation under grant no. CHE-0616340.

Supporting Information Available: Electronic absorption spectra for complexes **1**−**10** (Figure S1) and $Cu(phacac)_2$ (Figure S2), steady-state emission spectra for complexes **1**−**10** (Figure S3), time-resolved emission spectra for complexes **1**−**10** (Figure S4), and a complete listing of coauthors for ref 86. Crystallographic data for complexes **3** and **6** in cif format are also available. This material is available free of charge via the Internet at http://pubs.acs.org.

JA907303T